

Cell

microRNAs Establish and Maintain Uniform Cellular Phenotypes during the Architecture of Complex Tissues

--Manuscript Draft--

Manuscript Number:	
Full Title:	microRNAs Establish and Maintain Uniform Cellular Phenotypes during the Architecture of Complex Tissues
Article Type:	Research Article
Keywords:	microRNA; zebrafish mutant; phenotypic variability; cardiovascular development; endothelial cells; target gene networks
Corresponding Author:	Stefania Nicoli, PhD. Yale School of Medicine New Haven, CT UNITED STATES
First Author:	Dionna M Kasper
Order of Authors:	Dionna M Kasper Emma Ristori Albertomaria Moro Anand Narayanan Guillermina Hill-Teran Elizabeth Fleming Miguel Moreno-Mateos Charles Vejnár Jing Zhang Donghoon Lee Mengting Gu Mark Gerstein Stefania Nicoli, PhD. Antonio Giraldez
Abstract:	<p>Proper functioning of tissues requires cells to behave in uniform, well-organized ways. Conversely, many diseases involve increased cellular heterogeneity due to genetic and epigenetic alterations. Defining the mechanisms that counteract phenotypic variability is critical to understand how tissues sustain homeostasis. We performed a single-cell resolution screen of zebrafish embryonic blood vessels upon mutagenesis of single microRNA genes and multi-gene microRNA families. We found that microRNA mutants exhibit a profound increase in cellular phenotypic variability of vascular traits. Genome-wide analysis of endothelial microRNA target genes identified antagonistic regulatory nodes of vascular morphogenesis signaling that allow variable cell behaviors when derepressed. Remarkably, lack of microRNA activity sensitized vascular cells to microenvironmental changes induced by pharmacological stress. We uncover an unrecognized role of microRNAs as a widespread mechanism that limits variability in cellular phenotypes. This discovery marks an important advance in our comprehension of how microRNAs function in the physiology of higher organisms.</p>
Opposed Reviewers:	
Suggested Reviewers:	David Bartel dbartel@wi.mit.edu Richard Carthew r-carthew@northwestern.edu

	Alex Schier schier@fas.harvard.edu
	Stefan Schulte-Merker s.schulte@uni-muenster.de
	Deepak Srivastava dsrivastava@gladstone.ucsf.edu
	Brant Weinstein weinsteb@mail.nih.gov
	Leonard Zon zon@enders.tch.harvard.edu



Stefania Nicoli, Ph.D.
Assistant Professor
Department of Internal Medicine
Yale Cardiovascular Research Center
Office Room 773K, 300 George St.
New Haven, CT 06511
T 203 737-4151
stefania.nicoli@yale.edu

May 09, 2016

Subject: “**microRNAs Establish and Maintain Uniform Cellular Phenotypes During the Architecture of Complex Tissues**”

To the editorial board of Cell Journal,

Tissue and organ physiology is achieved by a collection of uniform cellular behaviors with optimal functionality. Determining how, molecularly, these normal phenotypes are precisely reproduced between individuals is fundamental to our understanding of organismal performance and ultimately disease susceptibility.

Here, we pinpoint miRNA regulation as one of the mechanisms adopted by higher organisms to establish and maintain phenotypic uniformity. Using single cell resolution screen of developing blood vessels in zebrafish, we show that disruption of miRNA-regulated networks led to a substantial increase in phenotypic variability of vascular traits, which resulted in sensitization to stress.

These findings represent significant **conceptual advances** over published literature. To date, only a single miRNA has been reported to prevent phenotypic variability such that it counteracted the effects of genomic variation on *Drosophila* scutellum bristle number (Cassidy et al., Cell 2013). Our data provide a deeper comprehension of this initial observation by demonstrating for the first time that:

1. miRNA regulation of phenotypic variability is a widely applicable mechanism, operating in multiple cellular contexts in vertebrate tissue.
2. Several miRNAs, including a multi-gene miRNA family, are necessary to limit phenotypic variability of specific developmental traits.
3. miRNAs have a broad protective function against diverse perturbations, not only limited to stress from genomic variation.

Additionally, our work has a **wide-reaching impact** for the following reasons:

1. We show that miRNA regulation of developmental networks is a general hallmark for tissue homeostasis. Since nearly all cell types are subject to phenotypic variability and express miRNAs, our data provide the framework for future and widespread mechanistic studies on how miRNA activity determines an individual's phenotype.
2. Although miRNAs are abundantly expressed throughout life, their loss has profound effects mainly in disease models. These counterintuitive findings have been difficult to reconcile in the history of miRNA biology. We uncover the missing link that miRNAs limit phenotypic variability in physiological settings as a way to prevent the impact of stress and consequently disease.

Because of all these reasons, we hope that you will consider the groundbreaking nature of our work for publication in Cell.

The following investigators are appropriate reviewers based on their fields of study in miRNA biology and cardiovascular development:

David Bartel	(dbartel@wi.mit.edu)
Richard Carthew	(r-carthew@northwestern.edu)
Alex Schier	(schier@fas.harvard.edu)
Stefan Schulte-Merker	(s.schulte@uni-muenster.de)
Deepak Srivastava	(dsrivastava@gladstone.ucsf.edu)
Brant Weinstein	(weinsteb@mail.nih.gov)
Leonard Zon	(zon@enders.tch.harvard.edu)

Sincerely,
Stefania Nicoli



microRNAs Establish and Maintain Uniform Cellular Phenotypes during the Architecture of Complex Tissues

Dionna M. Kasper¹, Emma Ristori¹, Albertomaria Moro¹, Anand Narayanan¹, Guillermina Hill-Teran¹, Elizabeth Fleming², Miguel Moreno-Mateos², Charles Vejnar², Jing Zhang^{5,6}, Donghoon Lee^{5,6}, Mengting Gu^{5,6}, Mark Gerstein^{5,6,7}, Antonio Giraldez^{2,3,4} and Stefania Nicoli^{1*}

¹Yale Cardiovascular Research Center, Department of Internal Medicine, Section of Cardiology, Yale University School of Medicine, New Haven, CT 06511, USA

²Department of Genetics, ³Yale Stem Cell Center, ⁴Yale Cancer Center, Yale University School of Medicine, New Haven, CT 06510, USA

⁵Program in Computational Biology and Bioinformatics, ⁶Department of Molecular Biophysics and Biochemistry, ⁷Department of Computer Science, Yale University, New Haven, CT 06520, USA

*Correspondence: stefania.nicoli@yale.edu

SUMMARY

Proper functioning of tissues requires cells to behave in uniform, well-organized ways. Conversely, many diseases involve increased cellular heterogeneity due to genetic and epigenetic alterations. Defining the mechanisms that counteract phenotypic variability is therefore critical to understand how tissues sustain homeostasis. Here, we carried out a single-cell resolution screen of zebrafish embryonic blood vessels upon mutagenesis of single microRNA (miRNA) genes and multi-gene miRNA families. We found that miRNA mutants exhibit a profound increase in cellular phenotypic variability of specific vascular traits. Genome-wide analysis of endothelial miRNA target genes identified antagonistic regulatory nodes of vascular growth and morphogenesis signaling that allow variable cell behaviors when derepressed. Remarkably, lack of such miRNA activity greatly sensitized the vascular system to microenvironmental changes induced by pharmacological stress. We uncover a previously unrecognized role of miRNAs as a widespread protective mechanism that limits variability in cellular phenotypes. This discovery marks an important advance in our comprehension of how miRNAs function in the physiology of higher organisms.

INTRODUCTION

How the genome creates reproducible phenotypes in the face of variable inputs is a fundamental question in biology. Biological systems constantly experience stochastic, genetic, and environmental variation. It has been proposed that mechanisms that tune transcript levels in response to such

perturbations are necessary to achieve phenotypic uniformity (Frankel et al., 2010; Ji et al., 2013; Raj et al., 2010; Staton et al., 2011). Impairment of these mechanisms in invertebrate development generates variable traits that are more susceptible to environmental changes (Cassidy et al., 2013; Rutherford and Lindquist, 1998). Unfortunately, whether these protective measures exist in higher organisms is completely unknown. Such a demonstration will reveal how complex sets of cells and tissues collectively achieve homeostasis. Furthermore, aberrant cell behaviors arising from errors in these mechanisms could greatly influence the effect of acquired risk factors on disease susceptibility. This will have a wide-reaching impact on how vertebrates establish and preserve phenotypes with optimal functionality.

One of the most abundant classes of gene regulatory molecules in vertebrates is miRNAs (Berezikov, 2011; Friedman et al., 2009). miRNAs silence gene expression by targeting messenger RNA (mRNA) for translational inhibition or decay (Bartel, 2009). The majority of protein-coding genes are controlled by miRNAs and a single miRNA can rapidly repress hundreds of transcripts (Baek et al., 2008; Selbach et al., 2008). miRNAs can collectively regulate positive and negative effectors of a genetic pathway, thereby providing precision to cellular behaviors (Choi et al., 2007b; Linsley et al., 2007). For these reasons, we propose miRNA-mediated gene silencing is one of the mechanisms that standardize phenotypes.

Here, we tested whether miRNAs regulate gene expression to counteract phenotypic diversity within a microenvironment. We used the zebrafish

cardiovascular system as a platform to probe the establishment and maintenance of endothelial cell phenotypes in the absence of miRNA activity. We analyzed three endothelial expressed miRNAs, and discovered that while all miRNA mutant populations displayed vascular cell-specific anomalies, only loss of some miRNAs resulted in increased variability of that trait. Furthermore, miRNA mutants with phenotypic heterogeneity were sensitized to perturbation by chemical drug treatment as they developed disease phenotypes. Genome-wide analyses of miRNA-target gene networks support a model by which miRNAs regulate pathways that are capable of counteracting the pharmacological stress. Our results provide the first evidence that vertebrate miRNAs are critical to limit phenotypic variability as a way to preserve tissue homeostasis.

RESULTS

Identification and mutagenesis of endothelial miRNAs

We used the zebrafish embryonic cardiovascular system to investigate a function for miRNAs in standardizing phenotypic expression. Cardiovascular phenotypes are easily detectable in this model due to the external growth and optical transparency of the embryo. These include the angiogenic sprouting of endothelial cells to form blood vessels beginning at ~24 hour post fertilization (hpf), hemogenic endothelium specification of hematopoietic stem/progenitor cells (HSPCs) starting at ~32 hpf, and vessel remodeling and maturation from 48 hpf to 6 days post fertilization (dpf) (Figure 1A) (Bertrand et al., 2010; Isogai et al., 2001; Isogai et al., 2003; Kissa and Herbomel, 2010). Using this well-

established platform, we first performed Illumina sequencing of miRNAs from endothelial (*Kdr1:GFP⁺*) and non-endothelial (*Kdr1:GFP⁻*) cells that were isolated from 24 hpf to 6 dpf embryos expressing the vascular-specific transgene *Tg(kdr1:gfp)^{la116}* (Figure 1A) . We found 46 miRNAs that were highly expressed and/or enriched in endothelial cells in at least one developmental stage, which we term “endothelial miRNAs” (Figures 1B and S1A).

To thoroughly assess the requirement of miRNAs in limiting phenotypic variability, we examined their function in three diverse vascular contexts. Specifically, we characterized single miRNA genes miR-139 and miR-223, as well as the miR-24 family, which is comprised of four genes that are processed into the same mature miRNA (Figure S1B). These miRNAs showed differential expression during vascular development as well as localization to different vascular beds (Figures 1B-1F). Specifically, we detected miR-139 in the trunk vasculature at 32 hpf by demonstrating the downregulation of mature miRNA levels in *etv2* morphant embryos, which lack intersegmental vessels (ISVs) (Figure 1D) (Pham et al., 2007). miR-24 expression at 54 hpf was limited to the ventral craniofacial region within pharyngeal arches, endoderm, and mesenchyme including the endothelium of the aortic arches. By 6 dpf, miR-24 became solely restricted to vascular cells (Figure 1E). miR-223 was observed in hemogenic endothelium along the ventral wall of the dorsal aorta (DA) at 32 hpf when HSPCs are specified, and at transient site of blood production at 54 hpf (Figure 1F) .

Next, we generated loss-of-function alleles to analyze the roles of miR-139, miR-24 family and miR-223. To form the functional ~22 base pair (bp) miRNA, the miRNA precursor transcript must be folded into a precise hairpin structure for Drosha/DGCR8 and Dicer cleavage (Ha and Kim, 2014). Therefore, we employed genome-editing techniques to induce mutations (referred to in the text as Δ) that interfere with miRNA processing as a way to disrupt miRNA activity (Figures 1G-1I and S1C). TAL effector nucleases (TALENs) produced a 9 Δ bp deletion in the miR-139 gene (Figure 1G) and two different 10 Δ bp and 8 Δ bp deletion alleles in miR-223 (Figure 1I). Additionally, injection of multiplexed pairs of CRISPR guide RNAs with Cas9 mRNA resulted in the concurrent mutagenesis of the four miR-24 family genes (Figure 1H). We analyzed mature miRNA levels in mutants homozygous for miR-139 (miR-139 Δ/Δ) and miR-223 (miR-223 Δ/Δ), and a miR-24 allelic series of 27 mutant genotypes derived from a miR-24-1+/ Δ 2+/ Δ 3+/ Δ 4 Δ/Δ incross (Figures 1K and S2). Mature miRNA expression was completely absent in miR-139 Δ/Δ and miR-223 Δ/Δ mutants, and was progressively diminished and ultimately lost from miR-24 single to quadruple mutants (Figures 1J-L). Thus, our generated alleles enabled loss of miRNA function studies.

Loss of miR-139 increases variability in endothelial cell shape phenotypes

Zebrafish miR-139 Δ/Δ mutants lacked obvious vascular morphological defects (e.g., pericardial edema and hemorrhaging) during embryonic development and were viable and fertile as adults (data not shown). Therefore,

we subjected maternal-zygotic miR-139 Δ/Δ embryos to a multifaceted screen with single-cell resolution for variation in specific cardiovascular traits (Figure S1D). While most markers and vessel growth were unaffected, we found an altered expression pattern for the chemokine receptor *cxcr4a* in ISVs of miR-139 Δ/Δ mutants at 32 hpf (Figures 2A-2D and S3A-C). Filopodia membrane extensions are numerous on endothelial cells during ISV formation and have been associated with chemokine regulated cell shapes (Isogai et al., 2001; Isogai et al., 2003; Meyen et al., 2015). As miR-139 was detected in ISVs (Figure 1D), we assessed filopodia morphology on single endothelial cells in these vessels. At 32 hpf, filopodia of cells lacking miR-139 activity were increased in number and longer in length compared to wild type cells on average (Figures 2E-2G). Strikingly, we also detected a greater variability of these cellular morphologies in miR-139 Δ/Δ mutants. While wild type endothelial cells possessed homogenous filopodia, miR-139 Δ/Δ cells ranged from lacking filopodia completely to having a multitude of filopodia of varying lengths as represented by the density distribution in the violin plots (Figures 2F and 2G). To quantify the variability in these phenotypic traits, we calculated the coefficient of variation and found a significantly higher value in miR-139 Δ/Δ compared to wild type embryos (Figures 2H and 2I). Thus, the more diverse spectrum of ISV endothelial cell shapes in miR-139 Δ/Δ embryos indeed resulted from changes in phenotypic variability.

In summary, although miR-139 Δ/Δ mutants exhibit ISV filopodia morphology similar by average to the wild type phenotypic optimum, they have the potential to explore a broader range of phenotypes despite a common

microenvironment (Figures 2J and 2K). In this fashion, miR-139 is required to standardize ISV endothelial cell shape.

Progressive loss of miR-24 enhances phenotypic variability in hypobranchial artery morphogenesis

Intrigued by the marked increase in variability of endothelial shape in miR-139 Δ/Δ embryos, we used our miR-24 allelic series derived from miR-24-1+/ Δ 2+/ Δ 3+/ Δ 4 Δ/Δ incrosses (Figures 1H and S2) to investigate whether miRNAs could promote phenotypic uniformity in a second vascular developmental context. Analysis of this vast collection of mutant genotypes also allowed us to explore how phenotypic heterogeneity responds to a step-wise loss of miRNA gene copies (Figure 1K).

All miR-24 Δ/Δ embryos, including quadruple mutants, lacked gross morphological defects and were viable at least through 6 dpf (Figures S4A and S4B). Therefore, we proceeded to screen miR-24 mutants with markers of the vasculature as well as craniofacial morphology because miR-24 was localized to both aortic and pharyngeal arches at 54 hpf (Figure 1E). Patterns of *sox9a*⁺ chondrocyte progenitors and derived cartilaginous structures were unaffected in miR-24 mutant embryos, and thus ruled out a possible contribution of this miRNA to craniofacial skeletal formation (Figure 3A). Confocal analysis of the developing ventral head vasculature did unveil a requirement for miR-24 in the morphogenesis of the hypobranchial artery (HA), which together with the aortic arches, supplies blood to ventral craniofacial tissues (Crucke and Huysseune,

2013; Isogai et al., 2001). Embryos lacking at least three miR-24 copies exhibited partial HA sprouting at 54 hpf, and by 6 dpf had a hypoplastic HA and less complex aortic arches, which correlated well with diminishing mature miR-24 levels in these vessels (Figure 3B). Patterning of other cranial vessels was comparable between all the miR-24 mutant genotypes and wild type embryos (Figure S4C), which points to the specificity of the vascular defects detected in the mutant background.

While quantification of HA length in miR-24 Δ/Δ embryos showed a significant reduction in HA size only in the miR-24 triple and quadruple mutants, we found a marked increase in phenotypic heterogeneity prior to the appearance of the sprouting defect (Figures 3C and 3D). Progressive depletion and loss of miR-24 expression resulted in embryos with a continuum of phenotypes ranging from an absent to a properly formed HA. Remarkably, miR-24 double mutant embryos possess a HA of normal length on average, but have a significantly increased coefficient of variation. Therefore, the miR-24 expression level resulting from the loss of two miR-24 gene copies coincides with the onset of HA phenotypic variability (Figure 3D).

Gradual loss of miR-24 activity allows individuals in a population to explore a broader range of smaller HA sizes and increases the probability of these embryos to have a phenotypic value outside the wild type spectrum (Figure 3E). Taken together, miR-24 ensures reproducible HA vascular morphogenesis.

Loss of miR-223 impacts HSPC formation from hemogenic endothelial cells without a change in phenotypic variability

Our study of miR-139 and the miR-24 family provides compelling evidence that miRNAs limit the heterogeneity of phenotypic outcomes in vertebrate development. Therefore, we tested the generality of this miRNA function in a third vascular context by investigating miR-223 activity.

miR-223 Δ/Δ embryos did not have overt vascular anomalies and grew up as fertile adults (data not shown). Accordant with miR-223 expression in *kdrt*⁺ and *cmyb*⁺ hemogenic endothelium (Figures 1B, 1C, 1F and S5A), embryos lacking miR-223 showed an expansion of *cmyb*⁺ expression resulting from increased *kdrt*⁺ *cmyb*⁺ hemogenic endothelial cells (Figures 4A-D and S5B). Vascular markers were unaffected in mutant embryos indicating that this defect was restricted to hematopoiesis (Figure S5C). Interestingly, phenotypic variability for hemogenic endothelial cell number was not statistically different between wild type and miR-223 Δ/Δ embryos (Figure 4E).

Analysis of additional hematopoietic markers in miR-223 Δ/Δ embryos revealed an expansion of *pu.1*⁺ myeloid progenitors and their neutrophil descendants, but not other differentiated blood cells (Figures 4F, 4G and S5D-5F). Again, the coefficient of variation of neutrophil number in miR-223 Δ/Δ mutants was proportional to that of wild type embryos (Figure 4H).

We conclude from these data that miR-223 regulates the formation of HSPCs from the hemogenic endothelium and their subsequent differentiation into specific myeloid cell types. Importantly, individuals lacking miR-223 do not

display increased variability as they have the same probability as wild type to explore a narrow spectrum of phenotypes in the two traits examined (Figure 4I and 4J). Thus, limiting phenotypic diversity is not a sole function for miRNAs during development.

Genome-wide analysis of miR-139, miR-24, and miR-223 endothelial target genes

To gain molecular insights into how miR-139, miR-24, and miR-223 differentially regulate phenotypes, we defined endothelial target gene networks individualized for each miRNA. We deep-sequenced polyadenylated RNAs in *Kdrl:GFP⁺* endothelial cells isolated from 24 hpf to 6 dpf *Tg(kdrl:gfp)^{la116}* embryos. From the endothelial transcripts identified, we determined the subsets that were classified as miRNA target genes by multiple prediction algorithms. Approximately 300 targets each, representing 9% of the developmentally expressed vascular genes, were assigned to miR-139, miR-24, and miR-223. We used the Circos software package to better visualize the regulatory activity of each miRNA. Links represent individual miRNA targets and point to their dynamic endothelial expression patterns between stages (Figure 5A). Consistent with their diverse functions, the majority of targets (colored links) for miR-139, miR-24, and miR-223 were uniquely regulated through vascular development, while only 30 endothelial transcripts were targeted by all three (grey links). Therefore, the defects observed in these miRNA mutants likely resulted from the disruption of a complex genetic network rather than a key target gene.

Examination of Gene Ontology (GO) terms demonstrated the functional relevance of the predicted endothelial miRNA targets to the observed vascular mutant phenotype (Figures 5B-5D). Significantly enriched GO terms for miR-139 and miR-24 included blood vessel development as well as terms associated with cell motility and migration such as small GTPase mediated signal transduction (Figures 5B-5C). In contrast, embryonic hematopoiesis was the most over-represented GO term for miR-223 (Figure 5D).

Many of the transcripts targeted by miR-139 and miR-24 have been empirically designated as pro-angiogenic or anti-angiogenic factors. Included in these genes were classic regulators of vascular growth and endothelial cell migration such as *flt1*, *plcγ*, and *amotl2a* for miR-139 and *ctnnb1*, *cdc42*, and *tie1* for miR-24 (Aase et al., 2007; Barry et al., 2015; Cattelino et al., 2003; Corada et al., 2010; Ernkvist et al., 2006; Fong et al., 1995; Krueger et al., 2011; Lawson et al., 2003; Li et al., 2010; Liao et al., 2002; Wakayama et al., 2015). Experimentally defined pro- and anti- hematopoietic factors were amongst miR-223 targets, including *myct1*, *jam3b*, and *aplrb* (Holmfeldt et al., 2016; Praetor et al., 2009; Yu et al., 2012). Strikingly, miRNA-target gene interaction maps describing these angiogenic or hematopoietic classifications were unexpectedly complex between miRNAs (Figures 5E-5G). Nearly all miR-223 targets corresponded to pro-hematopoietic genes (Figure 5G) while both pro- and anti-angiogenic genes were abundantly present in miR-139 and miR-24 networks (Figures 5E and 5F). Derepression of such interactions can originate in a broader

range of vascular growth and morphogenesis phenotypes detected in miR-139 and miR-24 mutants (Figures 2J, 2K and 3E).

Hence, a network comprised of opposing regulators is a unique signature of a miRNA limiting phenotypic variability.

Phenotypic heterogeneity in miRNA mutants confers sensitization to pharmacological stress

Mutations in miR-139 and the miR-24 family, but not miR-223 significantly impacted both vascular cell trait means and variability. However, as all the endothelial miRNA mutant embryos equally survived and did not experience adverse complications, the physiological requirement of these diverse modes of miRNA function were unclear. As previously suggested in invertebrates (Cassidy et al., 2013), we hypothesized that the phenotypic variability associated with miRNA loss might be the result of a genotype sensitized to variable perturbations. For this reason, we assessed the sensitization of miR-139, miR-24, and miR-223 mutants to a measurable environmental stress, in this case, a drug treatment. We chose stressors that would interfere with the respective miRNA-regulated cellular behaviors as they arise.

For miR-139, we selected the gamma secretase inhibitor IX (GSI), an antagonist of Notch signaling that interferes with ISV patterning (Figures 6A-6C) (Leslie et al., 2007). Strikingly, both miR-139^{+/ Δ} and miR-139 Δ/Δ genotypes manifested a significant abnormal number of ISV branches when exposed to a sub-dose of this drug that minimally perturbed control embryos (Figures 6A-6C).

Likewise, treatment with a sub-dose of Wnt signaling agonist 6-bromoindirubin-3'-oxime (BIO) induced shorter HA sprouts in all miR-24 mutant genotypes but not in control embryos (Figures 6D-6F). The profound anomalies dictated by minimum stressor exposure in miR-139 and miR-24 allelic series supported a true phenotypic sensitization of the mutant background rather than a simple genetic interaction between the miRNA and drug-signaling pathway. Consistent with our hypothesis, miR-223^{+/ Δ} and miR-223 Δ/Δ embryos were not sensitized to a sub-dose of S-Nitroso-N-acetyl-DL-penicillamine (SNAP), a nitric oxide donor that enhances HSPC formation (Figures 6G-6I) (North et al., 2009). The lack of drug sensitization could not be explained by a production limit in this cell type in the mutant background as miR-223 Δ/Δ embryos treated with SNAP displayed the expected enhancement of *kdr*⁺ *cmyb*⁺ hemogenic endothelial cells (Figure S6). Finally, coefficients of variation were consistently altered only in treated miR-139 and miR-24 mutants (Figures 6B, 6E and 6H).

Altogether, phenotypic variability associated with the loss of specific miRNA increased an individual's probability to develop disease-like phenotypes despite a common microenvironment (Figures 6C, 6F and 6I).

DISCUSSION

The physiology of tissues and organs is achieved by a collection of cell behaviors possessing a spectrum of phenotypes compatible with optimal functionality. How, molecularly, this spectrum is precisely reproduced between individuals is a fundamental question critical to our understanding of organismal

performance and ultimately disease. Here, we propose that miRNA-regulation of developmental networks is one mechanism adopted by vertebrates to establish and maintain phenotypic uniformity in the face of incoming variation from the microenvironment.

We used the developing zebrafish vasculature as a model to determine whether specific miRNAs are required for the standardization of endothelial cell behaviors. Isogenic miRNA mutant embryos lacking endothelial expressed miR-139 or miR-24 manifested measurable vascular phenotypic differences that were near the wild type optimum value, but occupied a wider range of phenotypic expression. As a consequence of the phenotypic variability, these genotypes were further sensitized to a discrete perturbation targeted to the specific miRNA controlled endothelial cell process. The progressive depletion of miRNA activity thereby increases the probability of embryos to possess heterogeneous phenotypes in both physiological and stress conditions. These results reveal an unrecognized function for miRNAs in vertebrates to limit congenital phenotypic heterogeneity and sensitization to acquired risk factors.

At the molecular level, our data support that miRNAs function as rheostats of developmental networks to allow phenotypic uniformity. Genome wide analysis for miR-139 and miR-24 target genes in vascular development revealed both positive and negative regulators of vessel growth and remodeling. Regulation of opposing activities is indicative of a position for miRNAs in feedback and feed forward homeostatic loops, which are well suited to respond to internal and external stimuli to maintain physiological functions (Ebert and Sharp, 2012; Ji et

al., 2013; Li et al., 2009; Tsang et al., 2007). Thus, involvement in such regulatory modes could explain why a loss of miR-139 and miR-24 activity led to a broad diversity of phenotypic outcomes outside the wild type limits.

In contrast to miR-139 and miR-24, depletion of miR-223 activity did not alter phenotypic trait variability in blood cell production. Accordingly, a notable difference in the miR-223 target gene network could explain this divergent function such that miR-223 almost exclusively targets transcripts that positively modulate hematopoiesis. Thus, the miR-223 regulated network is unable to counteract variable inputs as it lacked negative regulators to counterbalance a pro-hematopoietic program. Indeed, while miR-223 homozygous embryos possessed more hemogenic endothelial cells on average, the expression range of this phenotype was similar to that of wild type. Also, perturbation by a chemical stressor did not further increase HSPC formation in miR-223 genotypes. Since many other miRNAs are expressed in blood forming vascular cells (Nimmo et al., 2013), other miRNAs, rather than miR-223, could standardize this specific phenotype.

miRNAs are highly implicated in disease, however there has been no evidence connecting this relationship with congenital heterogeneity in cellular phenotypes. We believe our data provides the first example in vertebrates that miRNAs can developmentally program individuals to antagonize drug perturbation and potentially a broad range of other insults. Considering that the miRNAs studied here are highly conserved in mammals (Friedman et al., 2009), we speculate that this protective mechanism also exists in humans. Single

nucleotide polymorphisms (SNPs) in miRNA genes overlap nearly a thousand genomic regions linked to phenotypic variations, some of which have been verified experimentally to cause the specific trait heterogeneity (Amiel et al., 2012; Huan et al., 2015; Zorc et al., 2012). SNPs and mutations in miRNA genes and target binding sites are often associated with the probability to manifest a pathological condition such as carcinogenic transformation and cardiovascular disorders. Interestingly, the manifestation of such diseases is heterogeneous in the human population and clearly sensitive to risk factors, including genomic variation, age, and exposure to chemicals or other substances (Mendell and Olson, 2012; Quiat and Olson, 2013; Ryan et al., 2010). Our results would predict that individuals lacking specific miRNA activity could inherit a set of cellular phenotypes more prone to transformation or disease once exposed to a new environmental stress. In this respect, our discovery points to miRNA genetic variants as potential congenital markers that could instruct the management of susceptibility factors.

Even after twenty years of miRNA biology, it is still difficult to decipher the functions of specific miRNAs in the establishment of multicellular organisms, particularly in vertebrates (Lai, 2015). Only a handful of miRNAs are necessary for major developmental decisions and for viability, while most embryos lacking specific miRNA genes appear “normal” (Park et al., 2012; Vidigal and Ventura, 2015). Here, we present experimental evidence that helps to demystify this aspect of biology. We revealed a new mechanism in vertebrates by which miRNAs promote the uniformity of developmental traits as a way to limit the

impact of the environment on physiology. Since all cell types could be subject to phenotypic variability and regulation by miRNAs, our data provide the groundwork for widespread mechanistic studies on how miRNA regulation of developmental networks determines an individual's phenotype and disease susceptibility.

EXPERIMENTAL PROCEDURES

Detailed methods are available in Supplemental Experimental Procedures.

Zebrafish Strains and Husbandry

Zebrafish were raised and maintained using standard methods and according to protocols approved by Yale University Institutional Animal Care and Use Committee (# 2015-11473). Strains used in this study are AB wild type strain, *Tg(kdrl:gfp)^{la116}* (Choi et al., 2007a) and *Tg(kdrl:ras-mCherry)^{s896}* and *Tg(cmyb:GFP)^{zf169}* (Bertrand et al., 2010). See Supplemental Experimental Procedures for the generation of miR-139 and miR-223 mutants by TALEN mutagenesis and the miR-24 allelic series by CRISPR/Cas9 editing.

Identification of endothelial miRNAs and target genes

Endothelial cells were isolated by FACS from *Tg(kdrl:gfp)^{la116}* embryos at specified stages of cardiovascular development as described (Ristori and Nicoli,

2015). Small RNAs or polyadenylated mRNAs were extracted and deep sequenced on an Illumina platform. miRNAs that were highly expressed or enriched in endothelial cells were termed “endothelial miRNAs”. Transcripts with > 25 FPKM in endothelial cells and identified by at least two target prediction programs were considered miRNA target genes. See Supplemental Experimental Procedures for detailed RNA-seq protocols, as well as downstream network and Gene Ontology analyses.

Tol2 plasmid and Morpholino injections

Mosaic expression of the tol2-Fli1a-H2B-BFP-p2A-EGFP-Farnesyl vector in single endothelial cells was achieved by injecting single-cell embryos with 25 pg each of this plasmid and Tol2 transposase mRNA (Yu et al., 2015). One-cell embryos were injected with 2 ng of *tnnt2a* or control morpholino to stop blood flow (Packham et al., 2009) or with 5 ng of *etv2* or control morpholino to prevent ISV angiogenesis (Pham et al., 2007).

Chemical drug treatments

Embryos were treated with chemical compounds that interfere with the specific miRNA-regulated trait. To assay the effects of pharmacological stress on ISV morphogenesis, miR-139 mutant and wild type embryos were treated from 80% gastrula stage to 32 hpf with 50 or 100 μ M of gamma secretase inhibitor IX (Calbiochem) or with DMSO vehicle. The miR-24 allelic series and wild type embryos were treated from 48 to 54 hpf with 0.2 or 0.5 μ M (2'Z,3'E)-6-

Bromindirubin-3'-oxime (Enzo Life Sciences) to interfere with HA sprouting or with DMSO vehicle. 1 μ M or 10 μ M S-Nitroso-N-acetyl-DL-penicillamine (Sigma-Aldrich) was applied to miR-223 mutant and wild type embryos from 24 to 36 hpf to disrupt HSPC formation. All drug treatments were administered in egg water with 0.003% 1-phenyl-2-thiourea (PTU) to prevent pigmentation for downstream analyses, and stopped at the indicated time points by fixing embryos with 4% formaldehyde. Drug applications were carried out 2-3 times.

Northern blot analysis and qRT-PCR

Total RNA was extracted using TRIzol reagent (Life Technologies) according to the manufacturer's protocol. 3-5 μ g of total RNA was used for non-radioactive Northern blot analysis of miR-139 as described before (Nicoli et al., 2012). 0.5-1 μ g of total RNA was used for qRT-PCR analysis to measure relative miRNA and mRNA levels. See Supplemental Experimental Procedures for detailed protocols.

Whole mount *in situ* hybridization, immunohistochemistry and histological staining

WISH was carried out as previously described with minor modifications (Thisse and Thisse, 2008). 1:300 chicken anti-GFP (AbCam) primary and 1:400 Alexa Fluor 488 goat anti-chicken IgG (ThermoFisher) secondary antibodies were used in immunohistochemistry experiments. Sudan black, o-dianisidine, and alcian blue stainings were performed as described (Javidan and Schilling, 2004; Le

Guyader et al., 2008; Paffett-Lugassy and Zon, 2005). See Supplemental Experimental Procedures for elaborated protocols.

AUTHOR CONTRIBUTIONS

D.K. and S.N. designed and conducted experiments, analyzed data, and wrote the manuscript. E.R. carried out experiments and analyzed data. A.M. performed the computational and statistical analysis. J.Z., D.L., M.G., and M.G. computationally processed the raw RNA sequencing data sets. A.G. E.F, M.M-M and C.V. provided materials and reagents. A.N. and G.H-T. assembled and injected TALENs and CRISPR/Cas9. A.G, E.R. and A.M. edited the paper.

ACKNOWLEDGEMENTS

The authors would like to thank Hanna Mandl for technical assistance and Marie-Élise Schwartz and Meredith Cavanaugh for fish husbandry and care. We would also like to acknowledge Brant Weinstein for the H2B-farnesyl plasmid, and Trista North and Jenna Galloway for plasmids to make riboprobes. Finally, we are grateful to Hyung Joon Chun, Anne Eichmann, Karen Hirschi, Martin Schwartz, and Melanie Trombly for critical reading of the manuscript. This work was supported by grants from the NIH (R56A10087 and R01A10540 to S.N. and F32HL132475 to D.K.).

ACCESSION NUMBERS

RNA-seq experiments are submitted to the Gene Expression Omnibus

(<http://www.ncbi.nlm.nih.gov/geo/>).

SUPPLEMENTAL INFORMATION

Supplemental Information includes six figures, Supplemental Experimental Procedures, and Supplemental References.

REFERENCES

Aase, K., Ernkvist, M., Ebarasi, L., Jakobsson, L., Majumdar, A., Yi, C., Birot, O., Ming, Y., Kvanta, A., Edholm, D., *et al.* (2007). Angiomotin regulates endothelial cell migration during embryonic angiogenesis. *Genes & development* 21, 2055-2068.

Amiel, J., de Pontual, L., and Henrion-Caude, A. (2012). miRNA, development and disease. *Advances in genetics* 80, 1-36.

Baek, D., Villen, J., Shin, C., Camargo, F.D., Gygi, S.P., and Bartel, D.P. (2008). The impact of microRNAs on protein output. *Nature* 455, 64-71.

Barry, D.M., Xu, K., Meadows, S.M., Zheng, Y., Norden, P.R., Davis, G.E., and Cleaver, O. (2015). Cdc42 is required for cytoskeletal support of endothelial cell adhesion during blood vessel formation in mice. *Development* 142, 3058-3070.

Bartel, D.P. (2009). MicroRNAs: target recognition and regulatory functions. *Cell* 136, 215-233.

Berezikov, E. (2011). Evolution of microRNA diversity and regulation in animals. *Nature reviews Genetics* 12, 846-860.

Bertrand, J.Y., Chi, N.C., Santoso, B., Teng, S., Stainier, D.Y., and Traver, D. (2010). Haematopoietic stem cells derive directly from aortic endothelium during development. *Nature* 464, 108-111.

Cassidy, J.J., Jha, A.R., Posadas, D.M., Giri, R., Venken, K.J., Ji, J., Jiang, H., Bellen, H.J., White, K.P., and Carthew, R.W. (2013). miR-9a minimizes the phenotypic impact of genomic diversity by buffering a transcription factor. *Cell* 155, 1556-1567.

Cattellino, A., Liebner, S., Gallini, R., Zanetti, A., Balconi, G., Corsi, A., Bianco, P., Wolburg, H., Moore, R., Oreda, B., *et al.* (2003). The conditional inactivation

of the beta-catenin gene in endothelial cells causes a defective vascular pattern and increased vascular fragility. *J Cell Biol* 162, 1111-1122.

Choi, J., Dong, L., Ahn, J., Dao, D., Hammerschmidt, M., and Chen, J.N. (2007a). FoxH1 negatively modulates flk1 gene expression and vascular formation in zebrafish. *Developmental biology* 304, 735-744.

Choi, W.Y., Giraldez, A.J., and Schier, A.F. (2007b). Target protectors reveal dampening and balancing of Nodal agonist and antagonist by miR-430. *Science* 318, 271-274.

Corada, M., Nyqvist, D., Orsenigo, F., Caprini, A., Giampietro, C., Taketo, M.M., Iruela-Arispe, M.L., Adams, R.H., and Dejana, E. (2010). The Wnt/beta-catenin pathway modulates vascular remodeling and specification by upregulating Dll4/Notch signaling. *Developmental cell* 18, 938-949.

Crucke, J., and Huyseune, A. (2013). Unravelling the blood supply to the zebrafish pharyngeal jaws and teeth. *J Anat* 223, 399-409.

Ebert, M.S., and Sharp, P.A. (2012). Roles for microRNAs in conferring robustness to biological processes. *Cell* 149, 515-524.

Ernkvist, M., Aase, K., Ukomadu, C., Wohlschlegel, J., Blackman, R., Veitonmaki, N., Bratt, A., Dutta, A., and Holmgren, L. (2006). p130-angiomin associates to actin and controls endothelial cell shape. *FEBS J* 273, 2000-2011.

Fong, G.H., Rossant, J., Gertsenstein, M., and Breitman, M.L. (1995). Role of the Flt-1 receptor tyrosine kinase in regulating the assembly of vascular endothelium. *Nature* 376, 66-70.

Frankel, N., Davis, G.K., Vargas, D., Wang, S., Payre, F., and Stern, D.L. (2010). Phenotypic robustness conferred by apparently redundant transcriptional enhancers. *Nature* 466, 490-493.

Friedman, R.C., Farh, K.K., Burge, C.B., and Bartel, D.P. (2009). Most mammalian mRNAs are conserved targets of microRNAs. *Genome research* 19, 92-105.

Ha, M., and Kim, V.N. (2014). Regulation of microRNA biogenesis. *Nature reviews Molecular cell biology* 15, 509-524.

Holmfeldt, P., Ganuza, M., Marathe, H., He, B., Hall, T., Kang, G., Moen, J., Pardieck, J., Saulsberry, A.C., Cico, A., *et al.* (2016). Functional screen identifies regulators of murine hematopoietic stem cell repopulation. *J Exp Med* 213, 433-449.

Huan, T., Rong, J., Liu, C., Zhang, X., Tanriverdi, K., Joehanes, R., Chen, B.H., Murabito, J.M., Yao, C., Courchesne, P., *et al.* (2015). Genome-wide

identification of microRNA expression quantitative trait loci. *Nat Commun* 6, 6601.

Isogai, S., Horiguchi, M., and Weinstein, B.M. (2001). The vascular anatomy of the developing zebrafish: an atlas of embryonic and early larval development. *Developmental biology* 230, 278-301.

Isogai, S., Lawson, N.D., Torrealday, S., Horiguchi, M., and Weinstein, B.M. (2003). Angiogenic network formation in the developing vertebrate trunk. *Development* 130, 5281-5290.

Javidan, Y., and Schilling, T.F. (2004). Development of cartilage and bone. *Methods Cell Biol* 76, 415-436.

Ji, N., Middelkoop, T.C., Mentink, R.A., Betist, M.C., Tonegawa, S., Mooijman, D., Korswagen, H.C., and van Oudenaarden, A. (2013). Feedback control of gene expression variability in the *Caenorhabditis elegans* Wnt pathway. *Cell* 155, 869-880.

Kissa, K., and Herbomel, P. (2010). Blood stem cells emerge from aortic endothelium by a novel type of cell transition. *Nature* 464, 112-115.

Krueger, J., Liu, D., Scholz, K., Zimmer, A., Shi, Y., Klein, C., Siekmann, A., Schulte-Merker, S., Cudmore, M., Ahmed, A., *et al.* (2011). *Flt1* acts as a negative regulator of tip cell formation and branching morphogenesis in the zebrafish embryo. *Development* 138, 2111-2120.

Lai, E.C. (2015). Two decades of miRNA biology: lessons and challenges. *Rna* 21, 675-677.

Lawson, N.D., Mugford, J.W., Diamond, B.A., and Weinstein, B.M. (2003). phospholipase C gamma-1 is required downstream of vascular endothelial growth factor during arterial development. *Genes & development* 17, 1346-1351.

Le Guyader, D., Redd, M.J., Colucci-Guyon, E., Murayama, E., Kissa, K., Briolat, V., Mordelet, E., Zapata, A., Shinomiya, H., and Herbomel, P. (2008). Origins and unconventional behavior of neutrophils in developing zebrafish. *Blood* 111, 132-141.

Leslie, J.D., Ariza-McNaughton, L., Bermange, A.L., McAdow, R., Johnson, S.L., and Lewis, J. (2007). Endothelial signalling by the Notch ligand Delta-like 4 restricts angiogenesis. *Development* 134, 839-844.

Li, K., Blum, Y., Verma, A., Liu, Z., Pramanik, K., Leigh, N.R., Chun, C.Z., Samant, G.V., Zhao, B., Garnaas, M.K., *et al.* (2010). A noncoding antisense RNA in *tie-1* locus regulates *tie-1* function in vivo. *Blood* 115, 133-139.

Li, X., Cassidy, J.J., Reinke, C.A., Fischboeck, S., and Carthew, R.W. (2009). A microRNA imparts robustness against environmental fluctuation during development. *Cell* 137, 273-282.

Liao, H.J., Kume, T., McKay, C., Xu, M.J., Ihle, J.N., and Carpenter, G. (2002). Absence of erythropoiesis and vasculogenesis in *Plcg1*-deficient mice. *The Journal of biological chemistry* 277, 9335-9341.

Linsley, P.S., Schelter, J., Burchard, J., Kibukawa, M., Martin, M.M., Bartz, S.R., Johnson, J.M., Cummins, J.M., Raymond, C.K., Dai, H., *et al.* (2007). Transcripts targeted by the microRNA-16 family cooperatively regulate cell cycle progression. *Molecular and cellular biology* 27, 2240-2252.

Mendell, J.T., and Olson, E.N. (2012). MicroRNAs in stress signaling and human disease. *Cell* 148, 1172-1187.

Meyen, D., Tarbashevich, K., Banisch, T.U., Wittwer, C., Reichman-Fried, M., Maugis, B., Grimaldi, C., Messerschmidt, E.M., and Raz, E. (2015). Dynamic filopodia are required for chemokine-dependent intracellular polarization during guided cell migration in vivo. *Elife* 4.

Nicoli, S., Knyphausen, C.P., Zhu, L.J., Lakshmanan, A., and Lawson, N.D. (2012). miR-221 is required for endothelial tip cell behaviors during vascular development. *Developmental cell* 22, 418-429.

Nimmo, R., Ciau-Uitz, A., Ruiz-Herguido, C., Soneji, S., Bigas, A., Patient, R., and Enver, T. (2013). MiR-142-3p controls the specification of definitive hemangioblasts during ontogeny. *Developmental cell* 26, 237-249.

North, T.E., Goessling, W., Peeters, M., Li, P., Ceol, C., Lord, A.M., Weber, G.J., Harris, J., Cutting, C.C., Huang, P., *et al.* (2009). Hematopoietic stem cell development is dependent on blood flow. *Cell* 137, 736-748.

Packham, I.M., Gray, C., Heath, P.R., Hellewell, P.G., Ingham, P.W., Crossman, D.C., Milo, M., and Chico, T.J. (2009). Microarray profiling reveals *CXCR4a* is downregulated by blood flow in vivo and mediates collateral formation in zebrafish embryos. *Physiol Genomics* 38, 319-327.

Paffett-Lugassy, N.N., and Zon, L.I. (2005). Analysis of hematopoietic development in the zebrafish. *Methods Mol Med* 105, 171-198.

Park, C.Y., Jeker, L.T., Carver-Moore, K., Oh, A., Liu, H.J., Cameron, R., Richards, H., Li, Z., Adler, D., Yoshinaga, Y., *et al.* (2012). A resource for the conditional ablation of microRNAs in the mouse. *Cell Rep* 1, 385-391.

Pham, V.N., Lawson, N.D., Mugford, J.W., Dye, L., Castranova, D., Lo, B., and Weinstein, B.M. (2007). Combinatorial function of ETS transcription factors in the developing vasculature. *Developmental biology* 303, 772-783.

Praetor, A., McBride, J.M., Chiu, H., Rangell, L., Cabote, L., Lee, W.P., Cupp, J., Danilenko, D.M., and Fong, S. (2009). Genetic deletion of JAM-C reveals a role in myeloid progenitor generation. *Blood* 113, 1919-1928.

Quiat, D., and Olson, E.N. (2013). MicroRNAs in cardiovascular disease: from pathogenesis to prevention and treatment. *The Journal of clinical investigation* 123, 11-18.

Raj, A., Rifkin, S.A., Andersen, E., and van Oudenaarden, A. (2010). Variability in gene expression underlies incomplete penetrance. *Nature* 463, 913-918.

Ristori, E., and Nicoli, S. (2015). miRNAs expression profile in zebrafish developing vessels. *Methods in molecular biology* 1214, 129-150.

Rutherford, S.L., and Lindquist, S. (1998). Hsp90 as a capacitor for morphological evolution. *Nature* 396, 336-342.

Ryan, B.M., Robles, A.I., and Harris, C.C. (2010). Genetic variation in microRNA networks: the implications for cancer research. *Nat Rev Cancer* 10, 389-402.

Selbach, M., Schwanhausser, B., Thierfelder, N., Fang, Z., Khanin, R., and Rajewsky, N. (2008). Widespread changes in protein synthesis induced by microRNAs. *Nature* 455, 58-63.

Staton, A.A., Knaut, H., and Giraldez, A.J. (2011). miRNA regulation of Sdf1 chemokine signaling provides genetic robustness to germ cell migration. *Nature genetics* 43, 204-211.

Thisse, C., and Thisse, B. (2008). High-resolution in situ hybridization to whole-mount zebrafish embryos. *Nature protocols* 3, 59-69.

Tsang, J., Zhu, J., and van Oudenaarden, A. (2007). MicroRNA-mediated feedback and feedforward loops are recurrent network motifs in mammals. *Molecular cell* 26, 753-767.

Vidigal, J.A., and Ventura, A. (2015). The biological functions of miRNAs: lessons from in vivo studies. *Trends Cell Biol* 25, 137-147.

Wakayama, Y., Fukuhara, S., Ando, K., Matsuda, M., and Mochizuki, N. (2015). Cdc42 mediates Bmp-induced sprouting angiogenesis through Fmnl3-driven assembly of endothelial filopodia in zebrafish. *Developmental cell* 32, 109-122.

Yu, J.A., Castranova, D., Pham, V.N., and Weinstein, B.M. (2015). Single-cell analysis of endothelial morphogenesis in vivo. *Development* 142, 2951-2961.

Yu, Q.C., Hirst, C.E., Costa, M., Ng, E.S., Schiesser, J.V., Gertow, K., Stanley, E.G., and Elefanty, A.G. (2012). APELIN promotes hematopoiesis from human embryonic stem cells. *Blood* 119, 6243-6254.

Zorc, M., Skok, D.J., Godnic, I., Calin, G.A., Horvat, S., Jiang, Z., Dovic, P., and Kunej, T. (2012). Catalog of microRNA seed polymorphisms in vertebrates. *PloS one* 7, e30737.

FIGURE LEGENDS

Figure 1. Generation of endothelial miRNA mutants in zebrafish

(A) Experimental procedure to identify by Illumina sequencing miRNAs expressed in fluorescence activated cell (FAC)-sorted Kdr1:GFP⁺ endothelial cells and Kdr1:GFP⁻ non-endothelial cells during the four major stages of zebrafish vascular development. Dashed boxes outline the regions examined for cardiovascular phenotypes in endothelial miRNA mutant embryos (see Figure S1D).

(B) Heat map depicts miRNA reads per million in FAC-sorted Kdr1:GFP⁺ endothelial cells relative to non-endothelial for two biological replicates at the indicated stages for miR-139, miR-24, and miR-223. Color scale ranges from the first quartile (Q1) to the third quartile (Q3) fold enrichment values for all 46 endothelial miRNAs identified (see Figure S1A).

(C) Average mature miRNA levels relative to U6 snRNA expression as determined by quantitative reverse transcription polymerase chain reaction (qRT-PCR) in FAC-sorted Kdr1:GFP⁺ endothelial cells at the indicated developmental stages.

(D) Top, lateral trunk view of wild type embryos showing whole mount *in situ* hybridization (WISH) for mature miR-139, labeling cells within the ISV position. Confocal image shows the relative position of ISVs in the lateral trunk. Bottom, northern blot and respective quantification showing mature miR-139 expression relative to total RNA in three biological replicates of 32 hpf embryos treated as indicated.

(E) Mature miR-24 localization in the ventral head of wild type embryos in relation to *Kdr1*:GFP⁺ vasculature at the indicated developmental stages. By 6 dpf, miR-24 remained in vascular cells, but was excluded from cartilaginous and bone structures. Arrows point to anatomic landmarks. Yellow arrows point to the region captured in zoomed-in images.

(F) Mature miR-223 localization in the lateral *Kdr1*:GFP⁺ trunk vasculature of wild type embryos at the indicated stages. At 54 hpf, miR-223 is expressed in cells within the caudal hematopoietic tissue located between the DA and CV. Arrows show examples of miR-223⁺ cells. Yellow arrows point to the region captured in zoomed-in images.

(G-I) Schematic representation of the genome editing strategies employed to mutagenize endothelial miRNAs. TALENs for single miRNAs and a multiplexed CRISPR/Cas9 system for the miR-24 family were targeted to miRNA precursor genomic sequences to prevent mature miRNA formation. Grey boxes represent the wild type allele. Colored boxes reveal the nature of the mutant allele. See also Figure S1C.

(J-L) qRT-PCR showing average mature miRNA expression normalized to U6 snRNA levels in miRNA homozygous mutant embryos (J), embryo heads (K) or adult fins (L) relative to wild type. For miR-24 mutants, genotypes were categorized as a single mutant when two ($\Delta 2$, miR-24-4 Δ/Δ) and three ($\Delta 3$, ex. miR-24-1+/ Δ 4 Δ/Δ) miR-24 alleles were mutated, up to a quadruple mutant which lacked all eight miR-24 alleles ($\Delta 8$, miR-24-1 Δ/Δ 2 Δ/Δ 3 Δ/Δ 4 Δ/Δ). See also Figure S2.

Bar plots represent mean + S.E.M. and significance calculations were relative to wild type embryos. n.s. (not significant, $p > 0.05$), * $p \leq 0.05$, ** $p \leq 0.01$, and **** $p \leq 0.0001$, two-tailed Student's t test. qRT-PCR data represent 2-5 biological replicates, and 10-20 embryos from at least two different clutches were examined by WISH. Abbreviations: AA, aortic arches; DA, dorsal aorta; CV caudal vein; E, eye; EC, endothelial cell; H, heart; HA, hypobranchial artery; ISV, intersegmental vessel; PA, pharyngeal arch; PCV, posterior cardinal vein.

Figure 2. miR-139 homozygous mutants exhibit heterogeneity in endothelial cell shapes

(A) WISH of vascular angiogenesis marker *cxcr4a* in wild type and mutant embryos (n = 10-20). Yellow arrows in images (left) point to the ISVs captured in confocal projections that show *cxcr4a* within the lateral *Kdrl:GFP⁺* trunk vasculature (middle, right).

(B) Average fold expression of *cxcr4a* mRNA in miR-139 Δ/Δ tails normalized to *actb1* and relative to wild type tails at 32 hpf determined by qRT-PCR for 5 biological replicates.

(C) *cxcr4a* WISH and vessel morphology (arrows) in the lateral trunk of wild type and mutant embryos (n = 10-20). *cxcr4a* is expressed during sprouting angiogenesis at 26 hpf and downregulated in response to rapid blood flow by 54 hpf.

(D) Average ISV length was determined from confocal projections and is represented in terms of pixel number (n \geq 12).

(E) Representative images of single endothelial cells expressing tol2-Fli1a-H2B-BFP-p2A-EGFP-Farnesyl vector in wild type and miR-139 Δ/Δ ISVs. Endothelial cell nuclei are in blue (H2B-BFP) and membranes are in green (EGFP-Farnesyl).

(F-G) Phenotypic variability of endothelial cell shapes attributes, filopodia number (F) and length (G) is depicted with a violin plot (n = 14 cells). Violin plots show probability density. Dashed and dotted lines in box plots show mean and median values, respectively.

(H-I) Bars show quantification of phenotypic variability for filopodia number (H) and length (I) as determined by the coefficient of variation.

(J-K) Evidence-based models showing the probability density curves for filopodia number and length under a normal distribution. Endothelial cell shape trait values that fall within three standard deviations of the mean define the wild type phenotypic spectrum shaded in white. Values that deviate from this physiological range are in blue colored regions.

Bar plots show mean + S.E.M. and significance calculations were relative to wild type embryos. n.s. (not significant, $p > 0.05$), $*p \leq 0.05$, two-tailed Student's t test.

Abbreviations as defined in Figure 1. See also Figure S3.

Figure 3. Enhanced phenotypic variability in hypobranchial artery sprouting with diminishing miR-24 activity

(A) WISH of *sox9a* mRNA labeling chondrocyte progenitors (left) and alcian blue staining of cartilage (right) in the ventral head of wild type and miR-24 mutant embryos (n \geq 6 for all genotypes except n = 2 for quadruple mutants). Numbers

indicate the position of pharyngeal arches 1-7. miR-24 genotypes are categorized as in Figures 1K and S2.

(B) Ventral view of *Kdrl:GFP⁺* head vasculature. Arrows point to anatomic landmarks. Yellow arrows point to the HA sprout that is captured in zoomed-in images. Far right images show diminishing mature miR-24 expression in the aortic arches (AA) of the miR-24 allelic series.

(C) Quantification of HA length at 54 hpf from confocal projections (B) in terms of pixel number ($n = 12-18$ for all genotypes except $n = 5-6$ for quadruple mutants). Violin plots show HA length probability density. Dashed and solid lines in box plots are mean and median values, respectively.

(D) Coefficient of variation for HA length. Bars are mean + S.E.M.

(E) Evidence driven model showing the probability density curve for HA length under a normal distribution. HA length measurements that fall within three standard deviations of the mean determine the wild type phenotypic spectrum colored white. Values outside the wild type range are in blue shaded regions. Significance calculations were relative to wild type embryos. n.s. (not significant, $p > 0.05$), $*p \leq 0.05$, $**p \leq 0.01$, $***p \leq 0.001$, two-tailed Student's t test. See also Figure S4.

Figure 4. miR-223 does not regulate phenotypic variability of blood cell production

(A) WISH of HSPC marker *cmyb* at sites of hematopoiesis, namely the DA ventral wall at 32 hpf and the caudal hematopoietic tissue between the DA and

CV at 54 hpf (n = 10-20). Arrows show examples of *cmyb*⁺ cells. Yellow arrows indicate the region of the lateral trunk that is depicted in zoomed-in images.

(B) Mean *cmyb* expression in miR-223 Δ/Δ embryos normalized to *actb1* levels and compared to wild type as determined by qRT-PCR for three biological replicates.

(C) Representative confocal micrographs of the lateral trunk in embryos expressing *Tg(kdrl:ras-mCherry)*^{s896} and *Tg(cmyb:GFP)*^{zf169}. Arrows point to examples of *kdrl*⁺ *cmyb*⁺ hemogenic endothelial cells budding from the DA ventral wall at the peak of hematopoiesis. Yellow arrows show region of the lateral trunk that is captured in zoomed-in images.

(D) Quantification of *kdrl*⁺ *cmyb*⁺ hemogenic endothelial cells (n \geq 17). Violin representations show the probability density. Dashed and solid lines in box plots are mean and median values, respectively.

(E) Coefficient of variation for *kdrl*⁺ *cmyb*⁺ cell counts.

(F) Representative sudan black staining of neutrophils in the caudal hematopoietic tissue (arrows). Yellow arrows show regions of the lateral trunk that are captured in zoomed-in images.

(G) Quantification of neutrophil cells (n \geq 30). Plots as in D.

(H) Coefficient of variation for neutrophil counts.

(I-J) Evidence-based models showing the probability density curves for blood cell counts under a normal distribution. Data points that fall within three standard deviations of the mean define the range for the wild type phenotype shaded in

white. Values that deviate from this physiological spectrum are in blue highlighted regions.

Bar plots show mean + S.E.M. and significance comparisons were made with wild type embryos. n.s. (not significant, $p > 0.05$), $*p \leq 0.05$, $**p \leq 0.01$, and $***p \leq 0.001$, two-tailed Student's t test. Abbreviations as defined in Figure 1. See also Figure S5.

Figure 5. Genome wide identification of vascular target gene networks regulated by endothelial miRNAs

(A) Circos plot representations depicting the dynamic regulation of miRNA target genes in endothelial cells during vascular development. In the brown sector, stage specific heat maps show overall expression levels of genes expressed in *Kdr1*:GFP⁺ endothelial cells with >25 FPKM (fragments per kilobase of exon per million mapped reads) in at least one developmental stage. Genes are ranked by their 24 hpf expression level and each tick represents 100 genes. Endothelial expressed genes targeted by each miRNA are depicted as links. Colored links are unique targets and grey links are shared targets between miR-139, miR-24, and miR-223. Links connect target gene expression levels to their changes in gene expression between subsequent stages, where red and blue bars show upregulation and downregulation, respectively. Differential gene expression patterns (colored sectors) for miR-139 (blue), miR-24 (red), and miR-223 (green) target genes are depicted.

(B-D) Bar plots of vascular target genes significantly enriched in Gene Ontology terms for each miRNA. Genes with $-\log_{10}$ (Enrichment P value < 0.05) are shown.

(E-G) Differentially expressed target genes relating to vascular growth and remodeling (E, F) and hematopoiesis (G). Color scale reflects \log_2 (fold change) in expression between developmental stages when the defect is first observed. Fold changes for miR-139 and miR-223 targets were 48 versus (vs.) 24 hpf, and for miR-24 targets were 72 vs. 48 hpf. Shape size corresponds to the relative expression level of target genes for miR-139 and miR-223 at 24 hpf and for miR-24 at 48 hpf. Pro- and anti- designations were assigned based on published literature.

Figure 6. Phenotypic heterogeneity increases susceptibility to a disease-like state upon drug treatment

(A) Representative images of the trunk vasculature in 54 hpf wild type and miR-139 mutant embryos treated with the Notch signaling inhibitor GSI or DMSO vehicle. Arrows point to ectopic ISV branches.

(B) Top, violin plots show probability density of ectopic ISV branch number ($n = 11$ for DMSO control, $n = 21-26$ for GSI-treated embryos). Dashed and solid lines in box plots are mean and median values, respectively. Bottom, coefficient of variation for ISV branch number.

(C) Evidence-based models showing the probability density curves for ISV branch number. White shaded regions in both plots show trait values that fall

within three standard deviations of the mean for the sub-dose of drug (GSI 50).

Values that deviate from this spectrum are in blue highlighted regions with the disease-like state determined by the effect of the high drug dose (GSI 100).

(D) Representative micrographs of HA sprouting (arrows) in 54 hpf wild type and miR-24 mutant embryos treated with Wnt agonist BIO or DMSO vehicle. See also Figure S2 for the miR-24 genotypes represented in each mutant category.

(E) HA length quantification and coefficient of variation as in B (n = 12-18 for all genotypes except n = 5-6 for quadruple mutants). S = single, D = double, T = triple, Q = quadruple mutant.

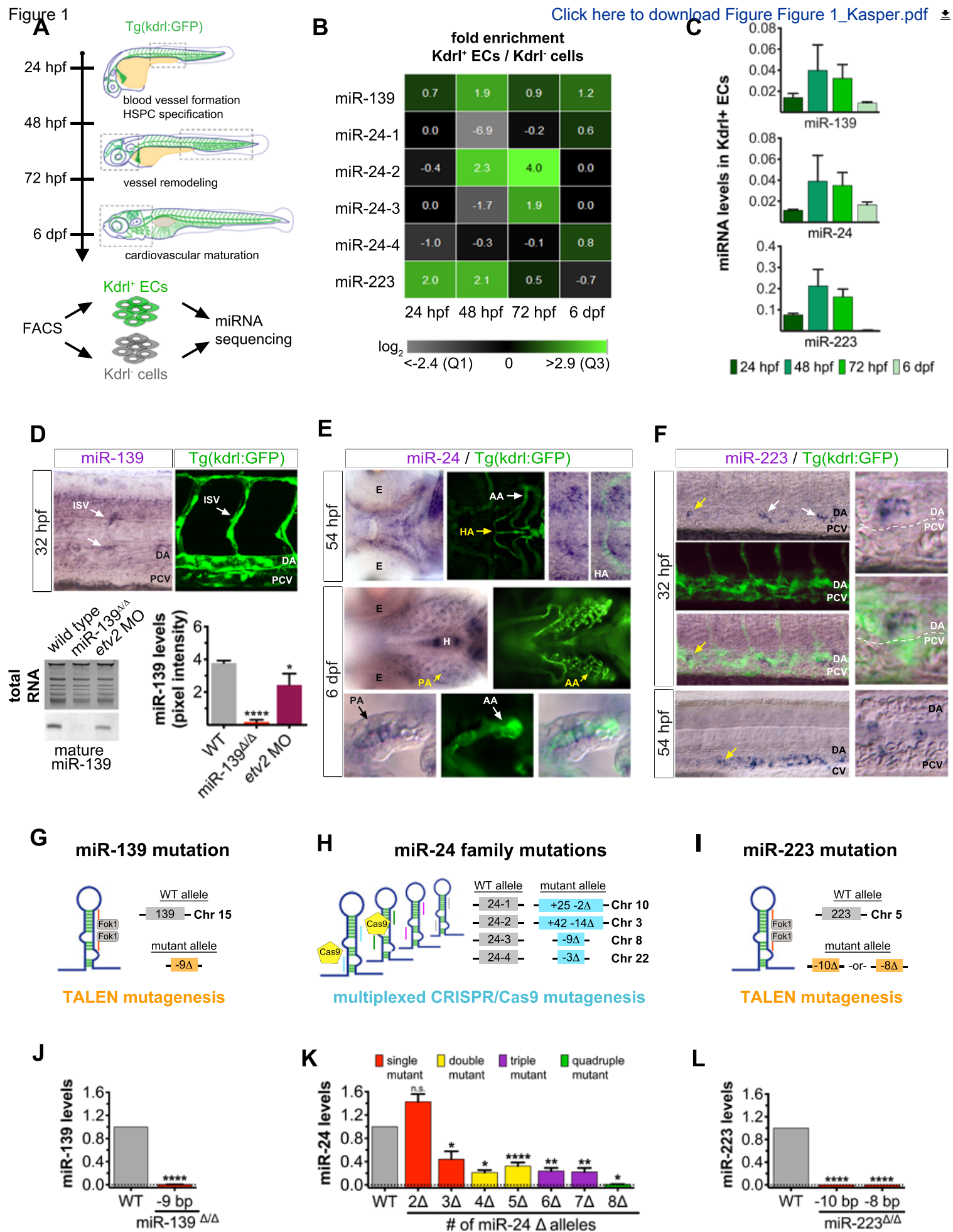
(F) Probability density curves for HA length as in C. Sub-dose of drug, BIO 0.2; high dose of drug, BIO 0.5.

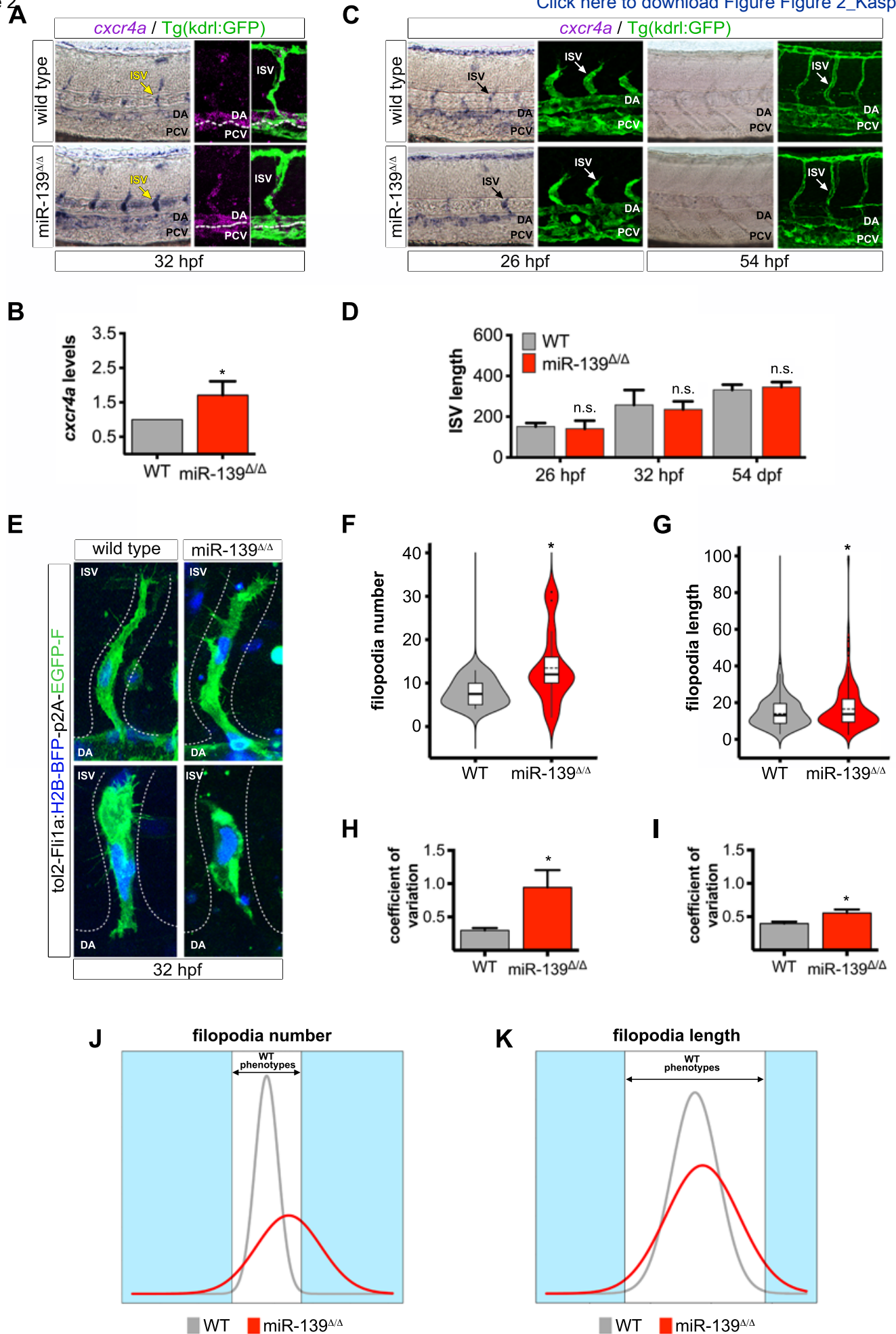
(G) Representative confocal projections showing *kdr*⁺ *cmyb*⁺ hemogenic endothelial cells (arrows) budding from the DA ventral wall in wild type and miR-223 mutant embryos untreated or treated with the NO donor SNAP at 36 hpf.

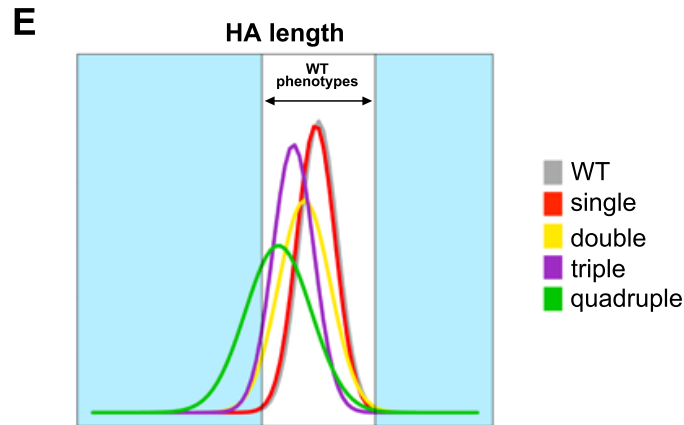
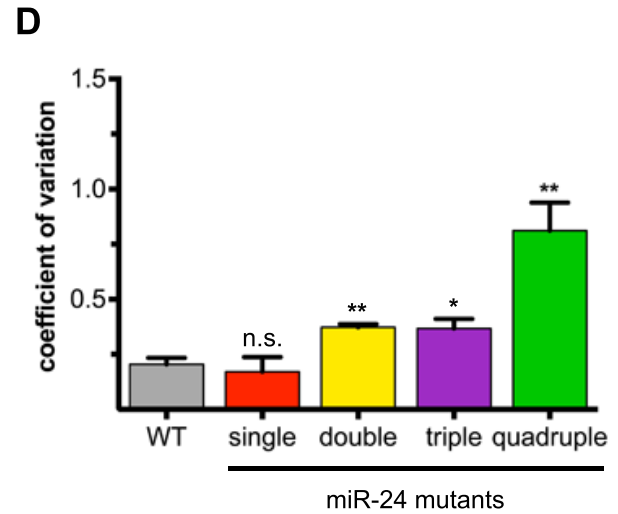
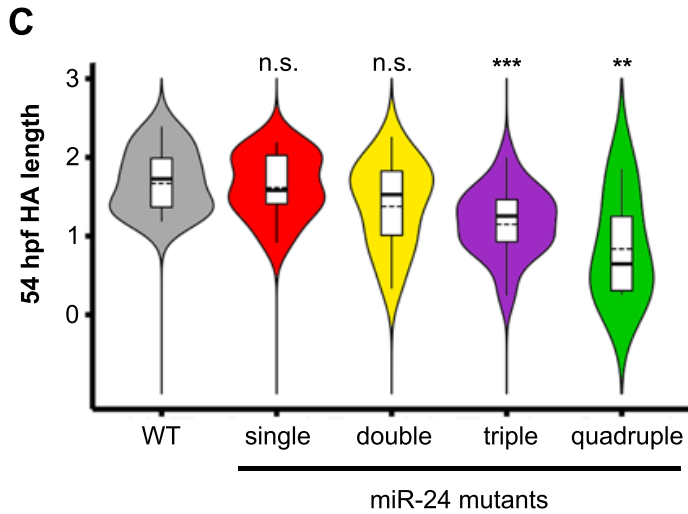
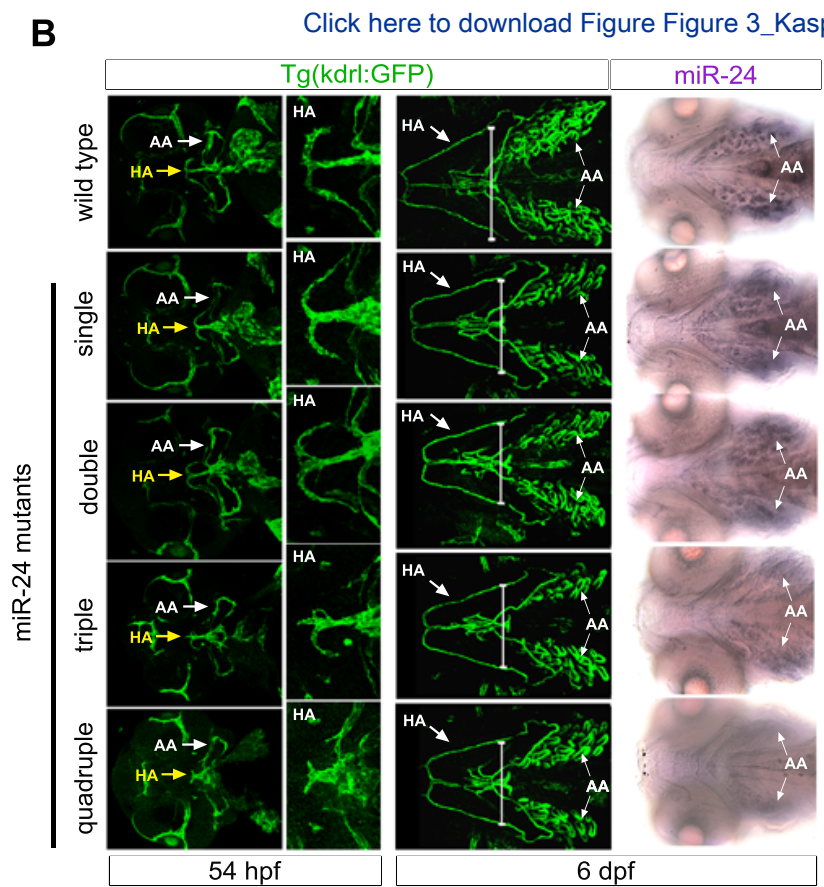
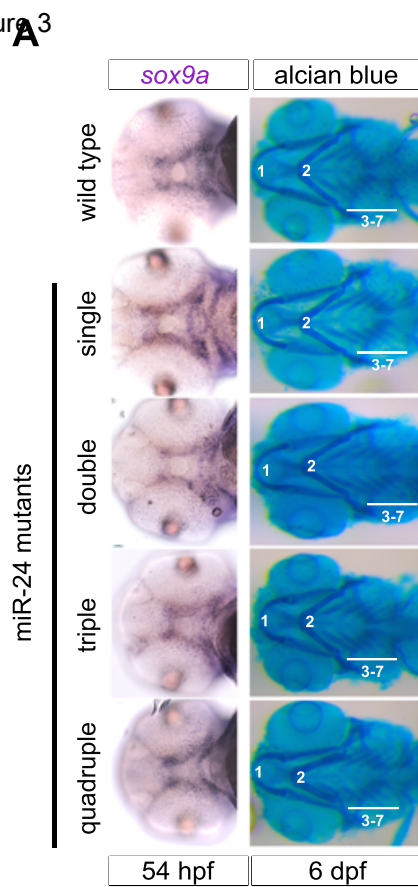
(H) Hemogenic endothelial cell counts and coefficient of variation as in B (n ≥ 17). UNT = untreated See also Figure S6.

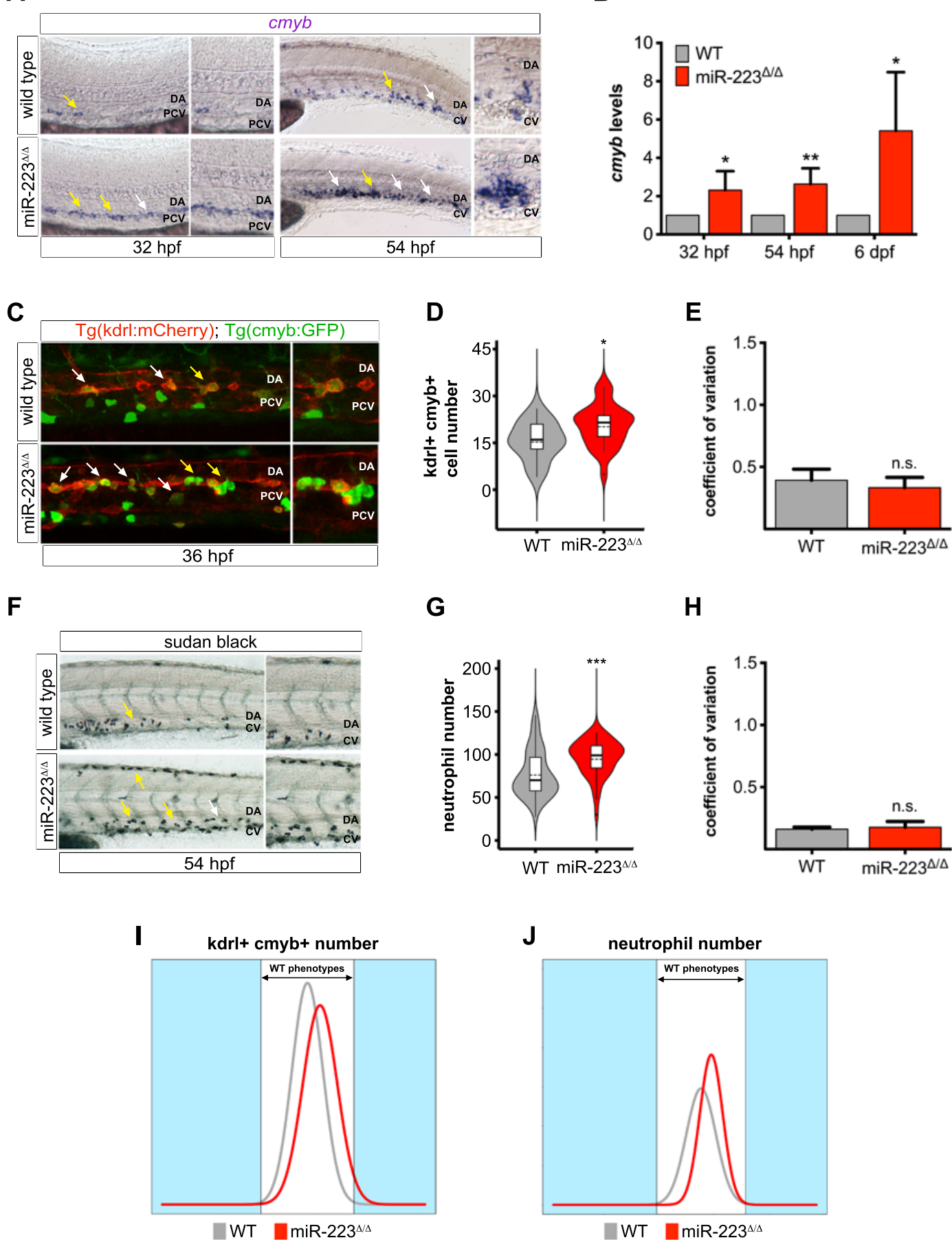
(I) Probability density curves for cell number as in C. Sub-dose of drug, SNAP 1; high dose of drug, SNAP 10.

For all bar plots, error bars show S.E.M. n.s. (not significant, $p > 0.05$), * $p \leq 0.05$, *** $p \leq 0.001$, and **** $p \leq 0.0001$, by two-tailed Student's t test.









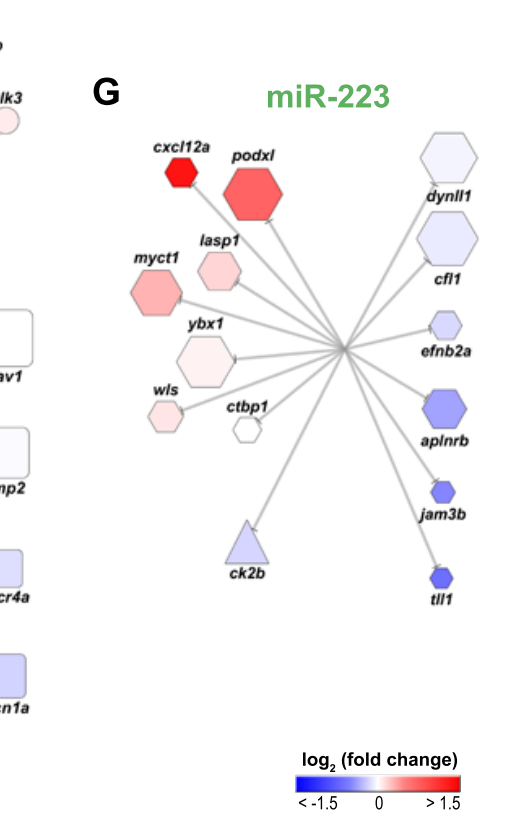
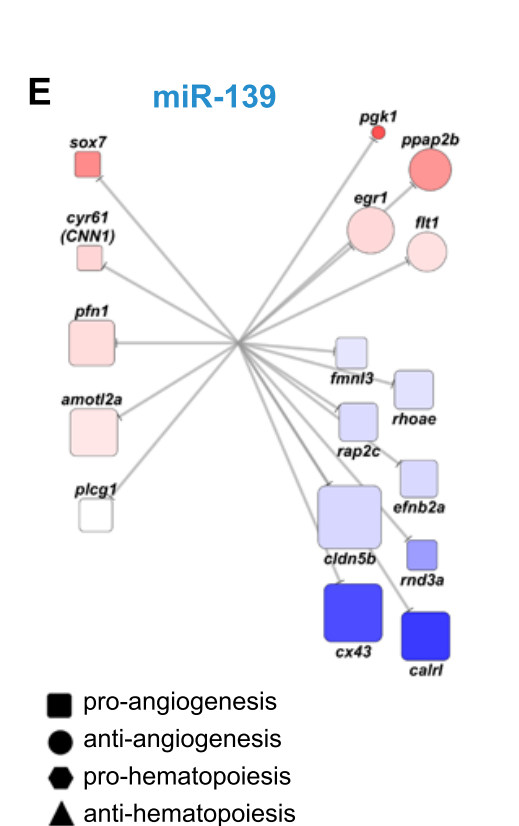
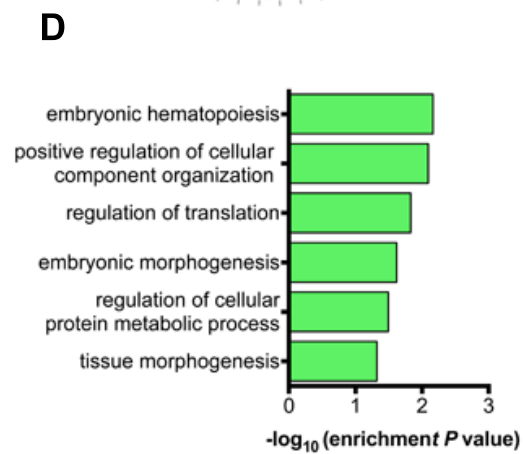
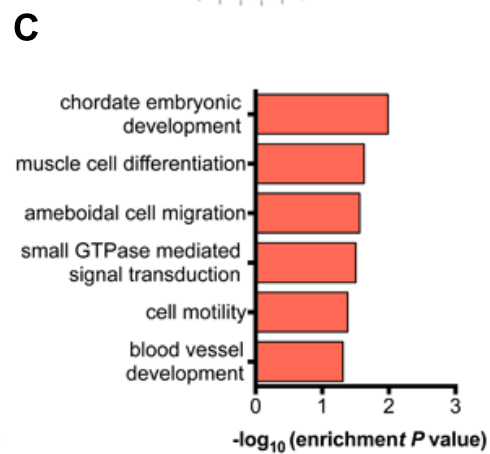
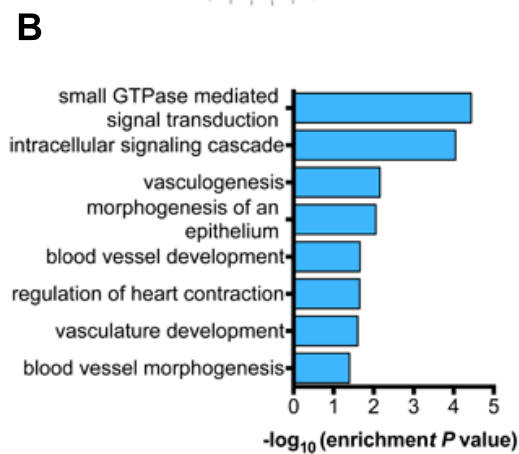
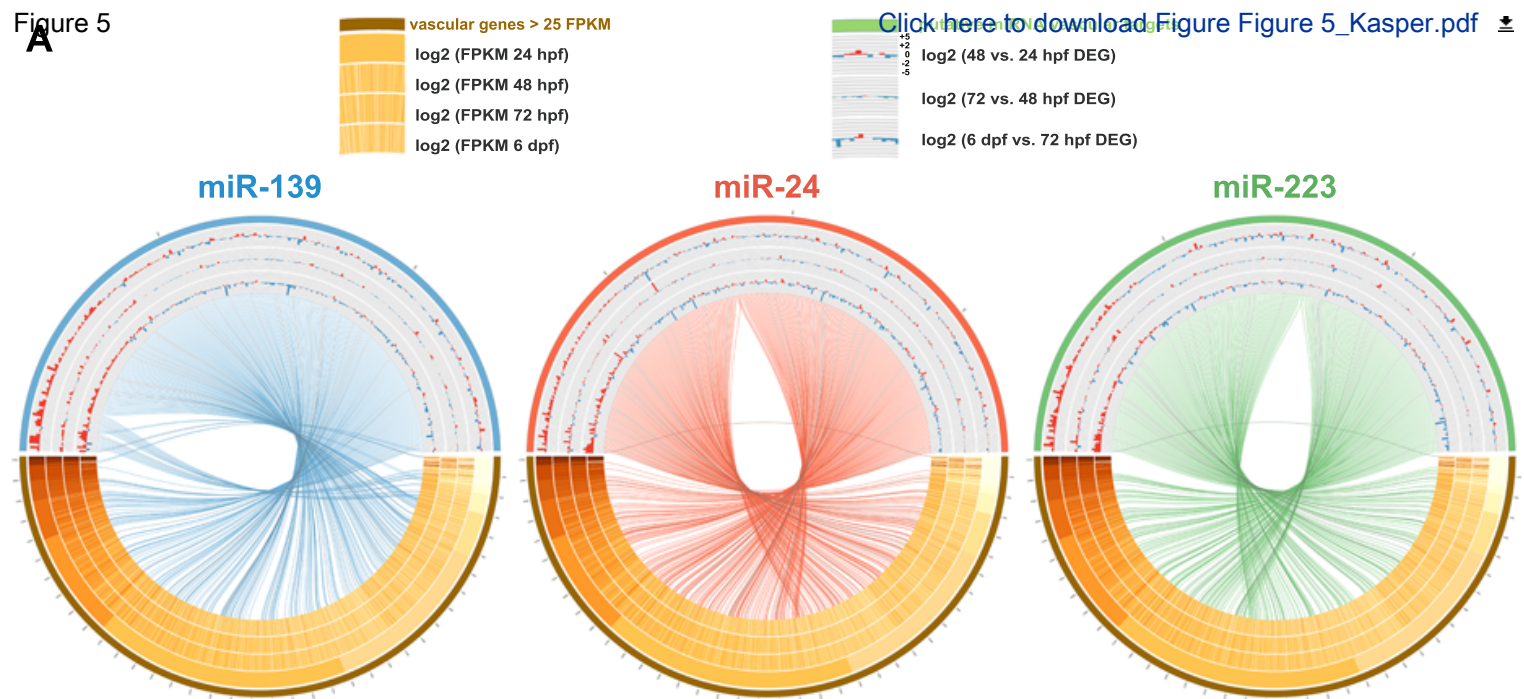
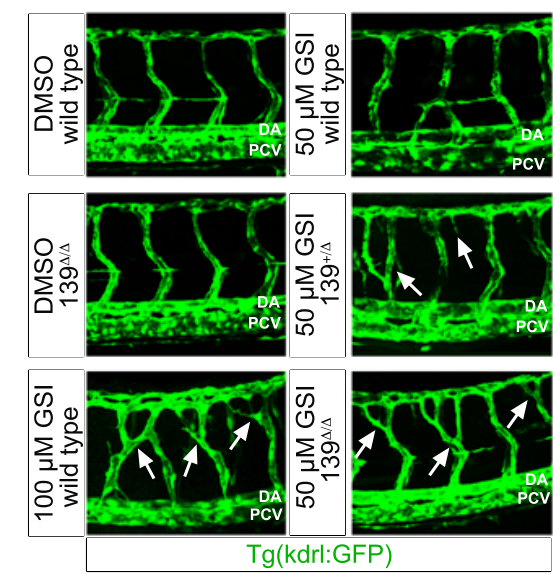
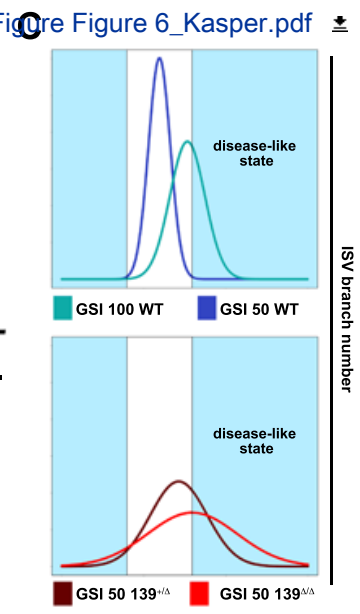
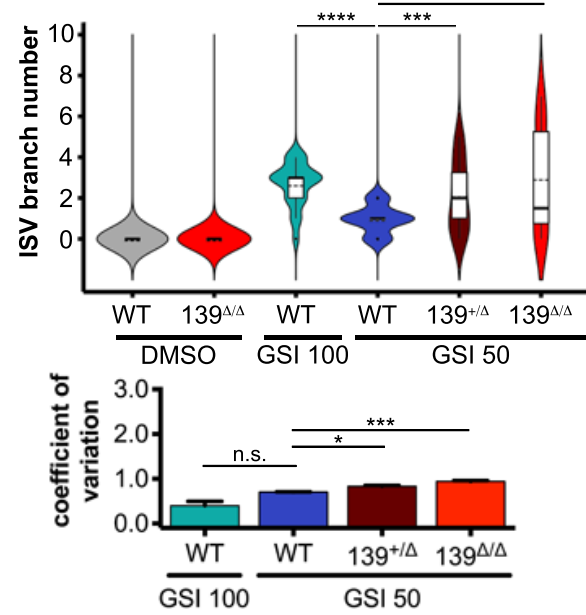
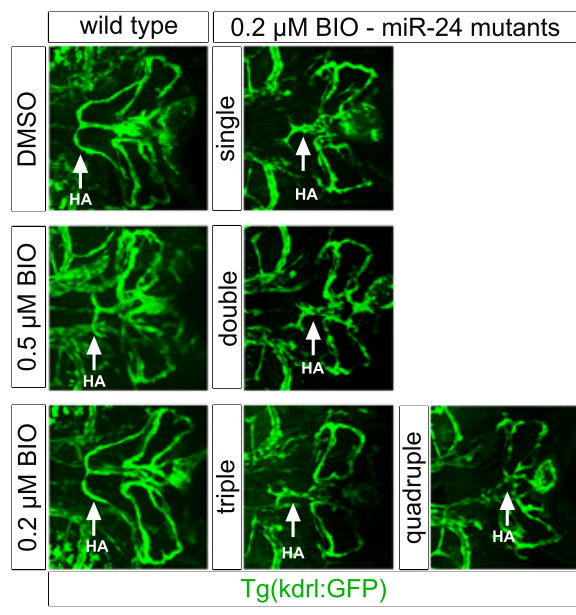
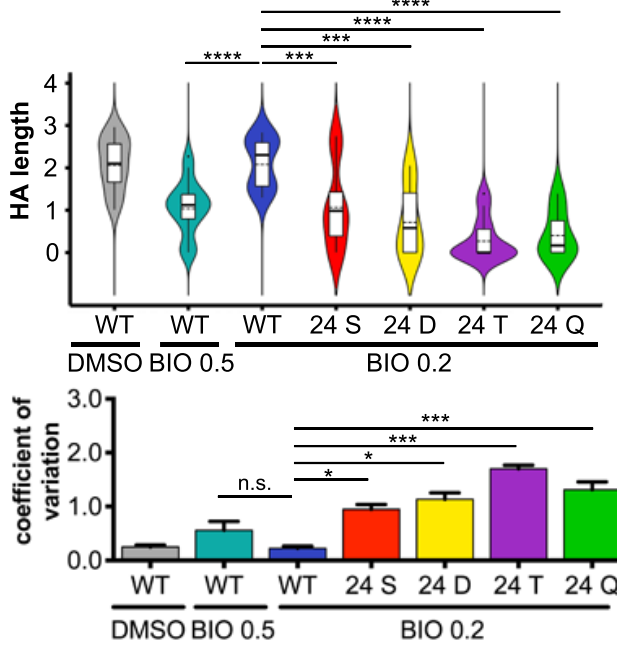
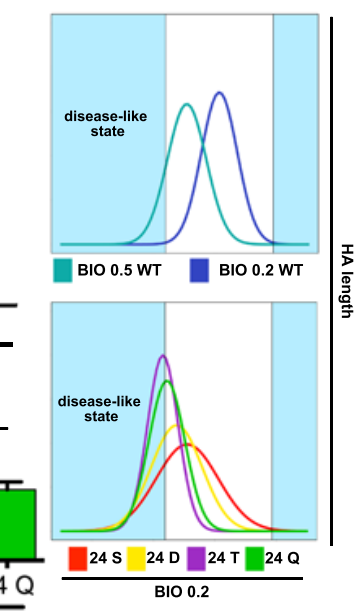
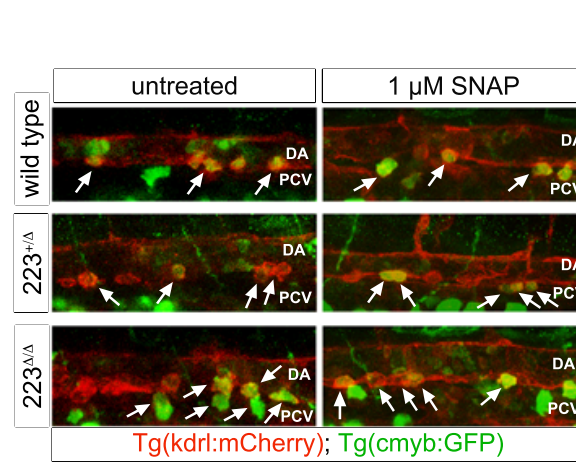
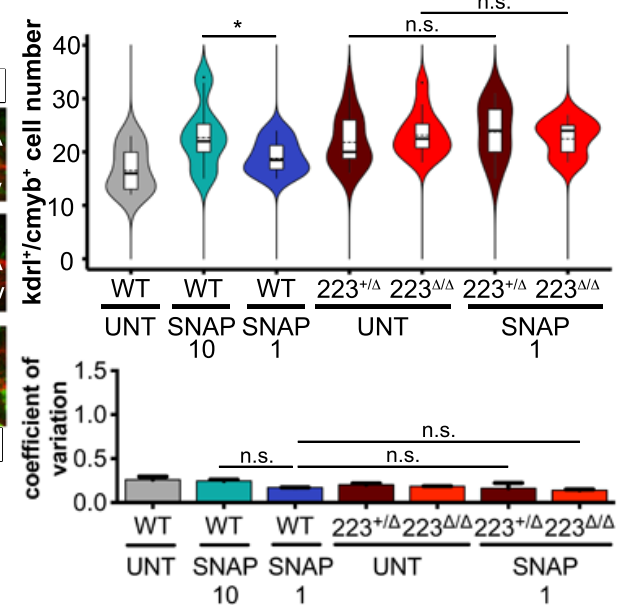
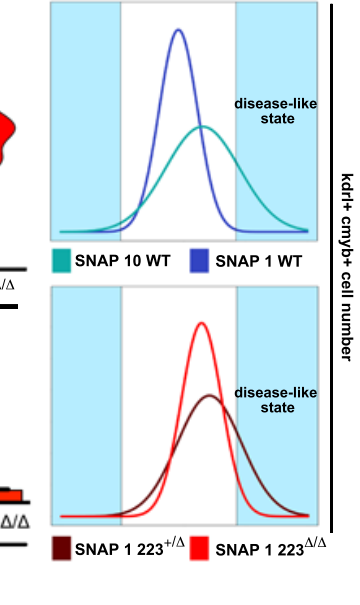


Figure 6**B****D****E****F****G****H****I**

SUPPLEMENTAL INFORMATION

microRNAs Establish and Maintain Uniform Cellular Phenotypes during the Architecture of Complex Tissues

Dionna M. Kasper, Emma Ristori, Albertomaria Moro, Anand Narayanan, Guillermina Hill-Teran, Elizabeth Fleming, Miguel Moreno-Mateos, Charles Vejnar, Jing Zhang, Donghoon Lee, Mengting Gu, Mark Gerstein, Antonio Giraldez, and Stefania Nicoli

Inventory of Supplemental Information

Supplemental Figures

Figure S1. Creation and reverse genetic screening of zebrafish endothelial miRNA mutants (related to Figure 1).

Figure S2. Classification of miR-24 genotypes (related to Figures 1, 3, and 6).

Figure S3. miR-139 does not regulate vessel outgrowth or flow-responsive processes (related to Figure 2).

Figure S4. miR-24 mutant embryos do not have delay in development (related to Figure 3).

Figure S5. miR-223 mutants have a specific defect in HSPC formation and neutrophil differentiation (related to Figure 4).

Figure S6. The HSPC production limit is not reached in miR-223 mutant embryos treated with SNAP (related to Figure 6).

Supplemental Experimental Procedures

Supplemental References

FIGURE S1
(related to Figure 1)

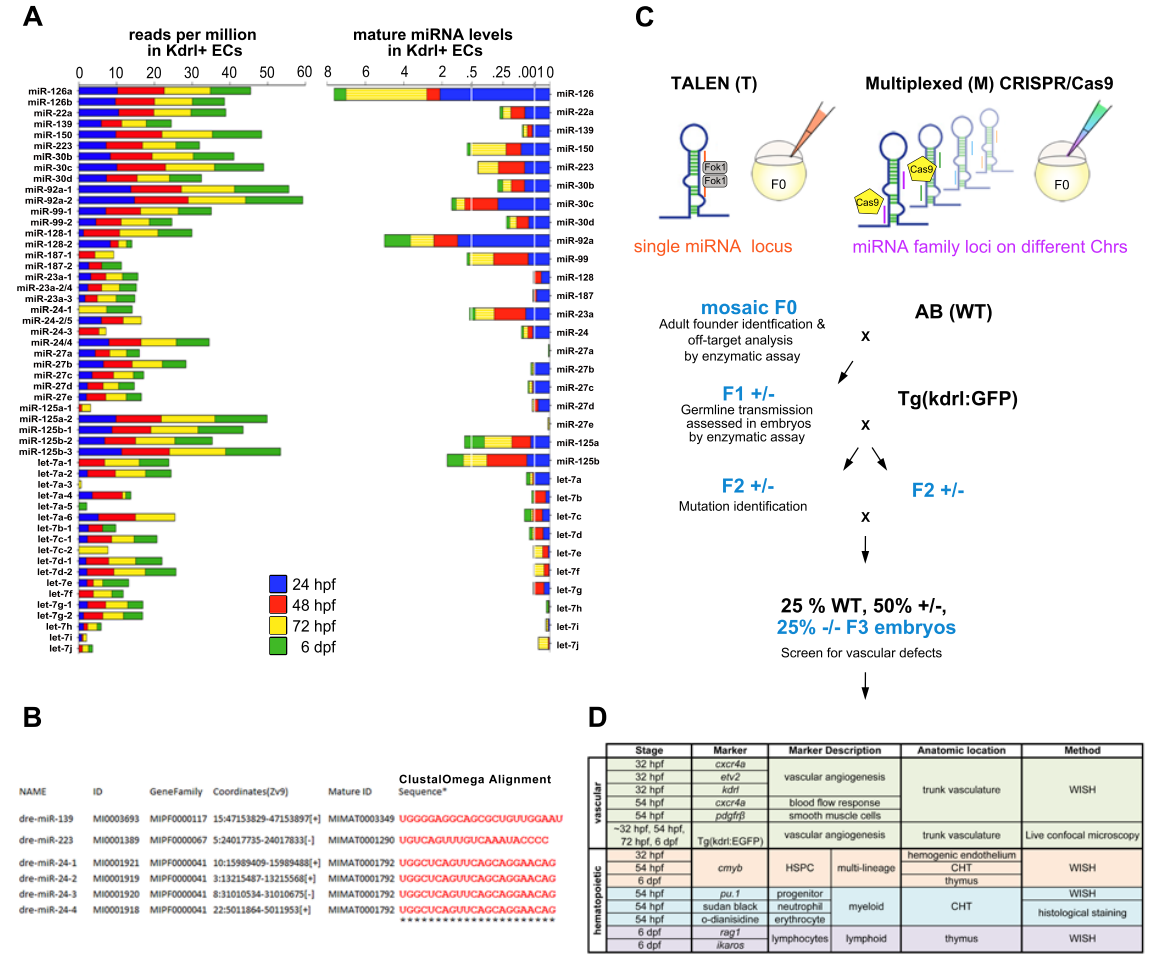


Figure S1. Creation and reverse genetic screening of zebrafish endothelial miRNA mutants (related to Figure 1).

(A) Left, sequencing reads per million for endothelial miRNAs expressed in cells FAC-sorted from *Tg(kdr1:gfp)^{la116}*. Right, average mature miRNA levels relative to U6 snRNA expression in *Kdr1:GFP⁺* endothelial cells as determined by qRT-PCR for two biological replicates. Developmental stages as indicated.

(B) Clustal Omega alignment of mature sequences for endothelial miRNAs characterized in this study.


(C) Single injection of one-cell zebrafish embryos with either TALENs or a multiplexed CRISPR guide RNA pool and Cas9 mRNA to mutagenize a single miRNA gene or multi-gene miRNA families, respectively. Founders were outcrossed first with the wild type AB strain and then with the *Tg(kdr1:gfp)^{la116}* strain to visualize the vasculature. Mutations in F0 were identified by an endonuclease assay, whereas mutations in subsequent generations were determined by fluorescent PCR fragment analysis. Embryos generated from F2 heterozygous in crosses were screened for cardiovascular defects as described in D.

(D) Table shows the markers and techniques used to screen zebrafish miRNA mutant embryos at the indicated stages. We evaluated endothelial-related processes including phenotypes involved in vascular development as well as definitive hematopoiesis due to the derivation of HSPCs from hemogenic endothelium. Abbreviations: CHT, caudal hematopoietic tissue; HSPC, hematopoietic stem and progenitor cell; WISH, whole mount *in situ* hybridization

FIGURE S2
(related to Figures 1, 3, and 6)

miR-24

1+/ Δ 2+/ Δ 3+/ Δ 4 Δ / Δ 1+/ Δ 2+/ Δ 3+/ Δ 4 Δ / Δ



# of MUTANT ALLELES	GENOTYPES	MUTANT CATEGORY
TWO	4 Δ / Δ	SINGLE
THREE	1+/ Δ , 4 Δ / Δ 2+/ Δ , 4 Δ / Δ 3+/ Δ , 4 Δ / Δ	SINGLE
FOUR	1 Δ / Δ , 4 Δ / Δ 2 Δ / Δ , 4 Δ / Δ 3 Δ / Δ , 4 Δ / Δ	DOUBLE
FIVE	1 Δ / Δ , 2+/ Δ , 4 Δ / Δ 1 Δ / Δ , 3+/ Δ , 4 Δ / Δ 1+/ Δ , 2 Δ / Δ , 4 Δ / Δ 1+/ Δ , 3 Δ / Δ , 4 Δ / Δ 2 Δ / Δ , 3+/ Δ , 4 Δ / Δ 2+/ Δ , 3 Δ / Δ , 4 Δ / Δ	DOUBLE
SIX	1 Δ / Δ , 2 Δ / Δ , 4 Δ / Δ 1 Δ / Δ , 3 Δ / Δ , 4 Δ / Δ 2 Δ / Δ , 3 Δ / Δ , 4 Δ / Δ	TRIPLE
SEVEN	1+/ Δ , 2 Δ / Δ , 3 Δ / Δ , 4 Δ / Δ 1 Δ / Δ , 2+/ Δ , 3 Δ / Δ , 4 Δ / Δ 1 Δ / Δ , 2 Δ / Δ , 3+/ Δ , 4 Δ / Δ	TRIPLE
EIGHT	1 Δ / Δ , 2 Δ / Δ , 3 Δ / Δ , 4 Δ / Δ	QUADRUPLE

Figure S2. Classification of miR-24 genotypes (related to Figures 1, 3, and 6).

Table lists the miR-24 genotypes evaluated for each mutant category. Genotypes with two or more heterozygous copies (ex. 1+/ Δ , 2+/ Δ , 3 Δ / Δ , 4 Δ / Δ) were excluded to simplify the interpretation of miR-24 mutant phenotypes.

FIGURE S3
(related to Figure 2)

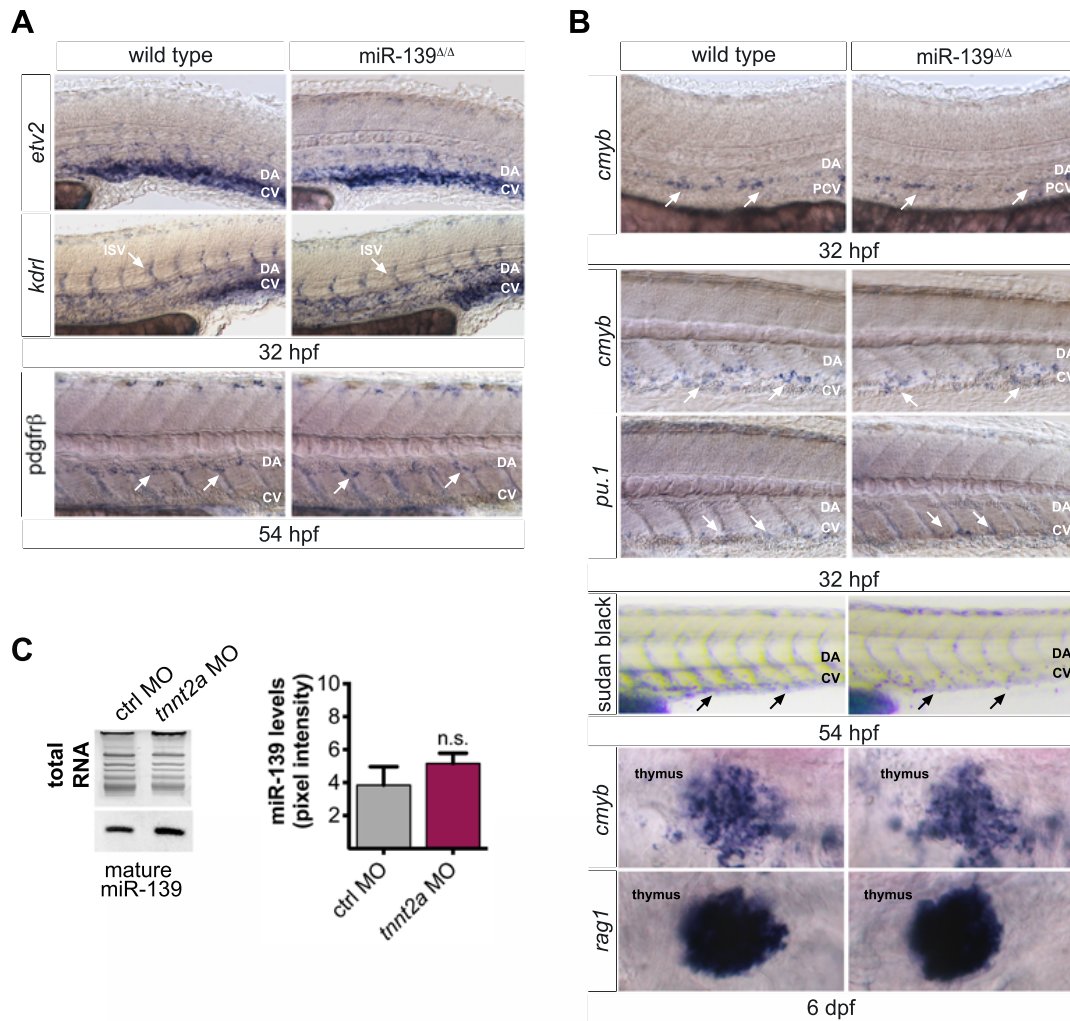


Figure S3. miR-139 does not regulate vessel outgrowth or flow-responsive processes (related to Figure 2).

(A) Lateral trunk view of WISH for angiogenesis markers *etv2* and *kdrl* and smooth muscle cell marker *pdgfrβ*. No differences were noted in mutant embryos.

(B) An increase in *cxc4a* expression can result from a moderate disruption in blood flow (Packham et al., 2009), so we examined WISH markers and sudan black staining for hematopoietic cells. Flow-dependent formation of *cmyb*⁺ HSPCs (North et al., 2009) and descending hematopoietic lineages were unaffected in miR-139^{Δ/Δ} embryos. *pu.1*⁺ progenitors and sudan black stained neutrophils were used to mark the myeloid lineage. *rag1* was used as a marker for lymphocytes.

(C) At 32 hpf, mature miR-139 expression was not statistically (n.s., $p > 0.05$.) different by two-tailed Student's t test in *tnnt2a* morphant embryos, which lack blood flow (Packham et al., 2009), compared to control morphant embryos with normal circulation. Northern blot quantification of mature miR-139 expression relative to total RNA. Bar plots show mean + S.E.M for three biological replicates.

For all images, arrows indicate representative staining and developmental stages are as indicated (n = 10-20 embryos).

FIGURE S4
(related to Figure 3)

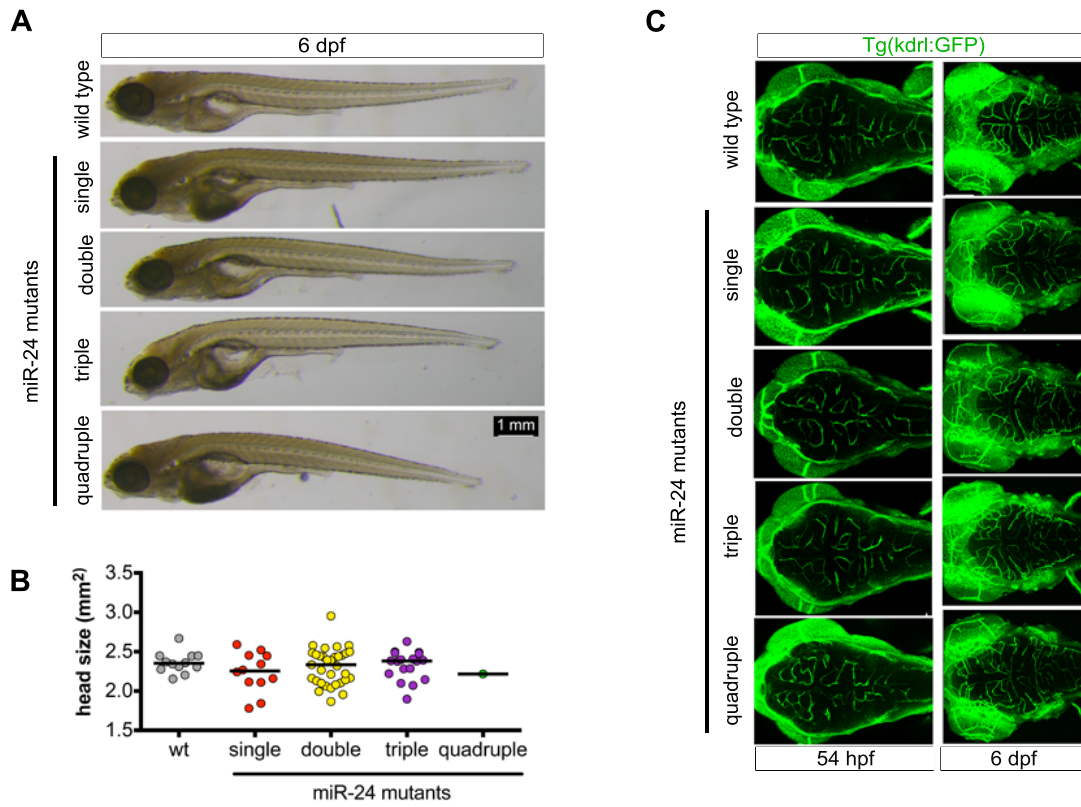


Figure S4. miR-24 mutant embryos do not have delay in development (related to Figure 3).

(A) Bright field images showing a representative lateral view of fixed wild type and miR-24 mutant embryos.

(B) Quantification of head area as a measure of overall growth. Solid line shows mean and data points are individual fish. Head size was not statistically different from wild type by two-tailed Student's t test.

(C) Dorsal view of central arteries in the *Kdrl:GFP*⁺ head vasculature.

FIGURE S5
(related to Figure 4)

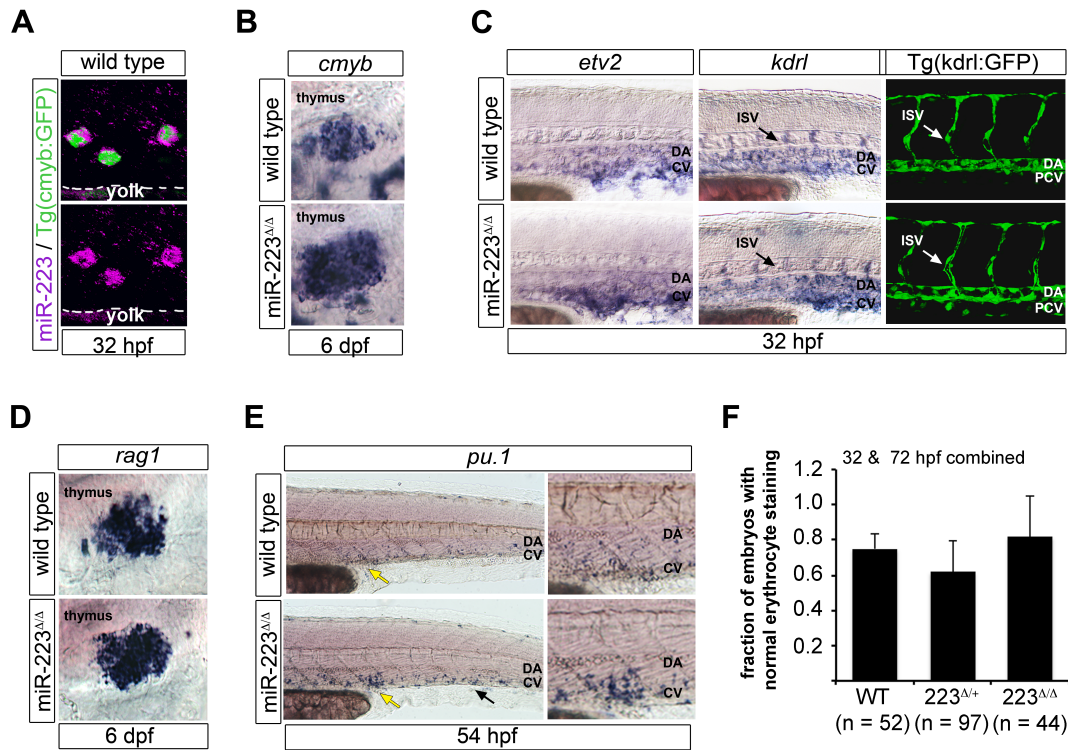


Figure S5. miR-223 mutants have a specific defect in HSPC formation and neutrophil differentiation (related to Figure 4).

(A) Confocal projection showing the localization of miR-223 WISH in *cmyb*:GFP⁺ HSPCs in the vasculature above the yolk extension.

(B) Lateral view of embryos showing *cmyb* mRNA localization in the thymus, a definitive site of hematopoiesis in zebrafish. Ectopic expression was visible in the miR-223 Δ/Δ embryos.

(C) WISH localization of vascular angiogenesis markers and vessel morphology revealed by *Tg(kdrl:gfp)^{la116}*. Arrows shows a positively stained ISV. No differences were detected between wild type and mutant embryos.

(D) WISH of lymphocyte marker *rag1* in the thymus was unaffected upon loss of miR-223.

(E) miR-223 Δ/Δ embryos exhibited an increase in *pu.1*⁺ myeloid progenitors in the caudal hematopoietic tissue (arrows), a transient site of hematopoiesis in the tail. Yellow arrows point to the region captured in zoomed-in images.

(F) Quantification shows the fraction of embryos with normal o-dianisidine staining of erythrocytes. Erythrocyte staining was not statistically different (n.s., $p > 0.05$) to wild type embryos by two-tailed Student's t test. Bars show mean + S.E.M.

For WISH and immunofluorescence experiments, n = 10-20 embryos.

FIGURE S6
(related to Figure 6)

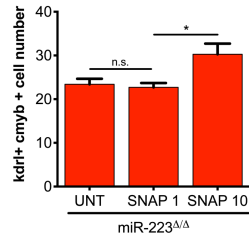


Figure S6. The HSPC production limit is not reached in miR-223 mutant embryos treated with SNAP (related to Figure 6).

Quantification of *kdr1*⁺ *cmyb*⁺ hemogenic endothelial cell number in 36 hpf miR-223 Δ/Δ embryos ($n \geq 17$). Bars show mean + S.E.M. Significance comparisons made with untreated (UNT) embryos. n.s. (not significant, $p > 0.05$) by two-tailed Student's t test.

SUPPLEMENTAL EXPERIMENTAL PROCEDURES

Identification of endothelial miRNAs

As previously described, *Kdrl:GFP*⁺ endothelial and *Kdrl:GFP*⁻ non-endothelial cells were isolated by FACS from *Tg(kdrl:gfp)*^{la116} embryos at 24 hpf, 48 hpf, 72 hpf and 6 dpf stages of cardiovascular development for two biological replicates. Total RNA was extracted from both FAC-sorted populations and used to prepare small RNA libraries for deep sequencing on an Illumina platform (Ristori and Nicoli, 2015). Adaptor sequences were trimmed off using Trimmomatic v 0.36, (Bolger et al., 2014) and resulting reads were mapped to the zebrafish Zv9 zebrafish genome version using RNA-STAR v.2.4 aligners (Dobin et al., 2013). Uniquely mapped small RNA-seq reads were counted at each gene locus, and normalized to total reads per million (RPM). We identified the most abundant and/or enriched miRNAs in endothelial cells, which we termed “endothelial miRNAs”. Abundant miRNAs were within the third quartile of the expression distribution for each stage of development in endothelial cells. Endothelial-enriched miRNAs had a greater than two fold average change in gene expression in endothelial compared to non-endothelial cells.

Generation of zebrafish endothelial miRNA mutants

As previously described, TALENs (Ristori et al., 2015) were used to create miR-139 and miR-223 mutants and a multiplexed pool of CRISPR guide RNA pairs and Cas9 mRNA (Moreno-Mateos et al., 2015) was used to simultaneously mutagenize all four miR-24 genes. Both strategies were carried out in the *Tg(kdrl:gfp)*^{la116} background. Mutagenesis was initially determined by restriction endonuclease assay using CviAII (NEB) for the miR-139 locus and T7 endonuclease I (NEB) for miR-24 and miR-223 genes. Briefly, 50 ng of genomic DNA isolated with the DNeasy Blood and Tissue kit (Qiagen) from a clutch of 15-20 injected 24 hpf embryos was used to amplify a 200-400 bp region spanning the intended mutation site. Differential restriction endonuclease patterns of PCR amplicons indicated successful genome editing. Once mutagenesis was confirmed, embryos remaining in the same clutch were raised. F0 founder fish were identified and outcrossed first with AB wild type and then with the *Tg(kdrl:gfp)*^{la116} strains to allow visualization of the developing vasculature. Mutations in adult F0 founders and subsequent generations were identified by 6-FAM fluorescent PCR fragment analysis. Genotyping PCR primers are listed in the table below. We characterized the nature of the mutant allele by cloning the mutant PCR product in a pGEM-T Easy vector (Promega) and sequencing the resulting plasmid.

Northern blot analysis and qRT-PCR

Total RNA from adult fin clips or pooled embryo heads, tails, or whole bodies was isolated using TRIzol reagent (Life Technologies) according to the manufacturer’s protocol. 3-5 µg of total RNA was used for non-radioactive Northern blot analysis of mature miRNA levels as described before (Nicoli et al., 2012). Hybridization of dre-miR-139 miRCURY LNA probe (Exiqon) occurred at 45°C. Pixel intensity of the mature miR-139 band was quantified using Image J software and normalized to the intensity of total RNA stained with ethidium bromide. Normalized mean miR-139 levels represent three biological replicates.

For quantification of small RNA levels, miScript II RT kit (Qiagen) was used to synthesize cDNA from 0.5-1 µg of total RNA according to the manufacturer’s protocol. miScript SYBER Green PCR kit (Qiagen) was performed as described by the manufacturer. Mature miRNA expression was normalized to U6 snRNA levels and relative to wild type. U6 primers (RNU6B, Hs_RNU6-2_1) were commercially provided from Qiagen. A similar procedure was followed to measure mRNA levels, except SuperScript III Reverse Transcriptase (Life Technologies) and KAPA SYBER FAST qPCR kit (Kapa Biosystems) were used instead. mRNA levels were normalized to the beta actin housekeeping gene, *actb1*. Reaction was according to the manufacturer’s protocol. All qPCR reactions were carried out in triplicate for 2-5 biological replicates in CFX96 Real-Time System thermal cycler (Bio-Rad). The $2^{-\Delta CT}$ or the $2^{-\Delta\Delta CT}$ methods were used to determine relative gene expression. qPCR primers are listed in the table below. miRNA universal reverse primer was provided by Qiagen.

Whole mount *in situ* hybridization, immunohistochemistry and histological staining

Embryos subjected to whole mount *in situ* hybridization (WISH), immunohistochemistry, and histological staining were raised in 0.003% PTU starting after the gastrulation stage to prevent pigmentation. Zebrafish embryo fixation with 4% formaldehyde and WISH were performed as previously described (Thisse and Thisse, 2008) with the following modifications. To detect mRNA expression, digoxigenin labeled

riboprobes were synthesized using a DIG RNA labeling kit (SP6/T7; Roche Applied Bioscience) and hybridized with embryos overnight at 60°C. To detect miRNA expression, double-digoxigenin labeled miRCURY LNA probe oligonucleotides (Exiqon) were hybridized overnight at 45-55°C. Post hybridization washes occurred at the hybridization temperature and consisted of 2 x 30 minutes (min.) 2x SSCTw/50% formamide washes, 1 x 30 min. 2x SSCTw wash, and 2 x 30 min. 0.2x SSCTw. After blocking in 5% sheep serum/PBSTw for at least 1 hour, embryos were incubated overnight at 4°C in 1:10,000 sheep anti-DIG AP Fab fragments (Roche) in blocking solution. The WISH signal was revealed with 1:50 dilution of NBT/BCIP (Roche) in alkaline phosphatase buffer. When immunohistochemistry was performed with WISH, 1:300 chicken anti-GFP (AbCam) primary antibody was incubated with anti-DIG AP and 1:400 Alexa Fluor 488 goat anti-chicken IgG (ThermoFisher) secondary antibody was applied as the last step after WISH development.

To better visualize *kdrl*+ *cmyb*+ hemogenic endothelial cells, immunohistochemistry was performed to amplify the *cmyb*:GFP signal as follows. After overnight 4% formaldehyde fixation at 4°C, embryos were washed 4-5x with PBSTw, and then washed 3-4 x 5 min. plus 2 hours in blocking solution (0.8% Triton-X, 10% normal goat serum, 1% BSA, 0.01% sodium azide in PBSTw. Concentrations of anti-GFP primary and Alexa Fluor 488 secondary antibodies are as above. Following overnight antibody incubation at 4°C, six washes for a total of 6 hours were performed with blocking solution lacking goat serum at room temperature.

Sudan black staining (Sigma-Aldrich) of neutrophils (Le Guyader et al., 2008) and o-dianisidine staining (Sigma-Aldrich) of erythrocytes (Paffett-Lugassy and Zon, 2005) was performed on at least 30 embryos per genotype from at least 3 separate clutches as previously reported. Alcian blue staining (Sigma-Aldrich) of cartilage (Javidan and Schilling, 2004) was performed on 2-3 independent clutches of at least 6 embryos per genotype except for quadruple mutants where 2 animals were examined.

Genomic DNA from whole or portions of embryos was extracted by boiling at 95°C for 20 minutes in 25-30 µl of 100 mM sodium hydroxide and then neutralized with ~10-12 µl of 1M Tris-HCl pH 7.5. 6-FAM fluorescent PCR was carried out with 1-3 µl of genomic DNA using genotyping primers in the table below and submitted for PCR fragment analysis.

The majority of fluorescent images were captured using a Leica Microsystems SP5 confocal microscope using a 25X objective except for images of single endothelial cells expressing H2B-BFP:EGFP-Farnesyl plasmid that were taken with a 40X objective. Max projections were generated with the Leica application suite or Perkin Elmer Velocity software. All differential interference contrast microscopy images and fluorescent images in Figures 1E and 1F were acquired with the Nikon Eclipse 80i microscope with a 20X objective.

WISH probe	Reference
<i>cxcr4a</i>	(Chong et al., 2001)
<i>cmyb</i>	(Murayama et al., 2006)
<i>etv2</i>	(Pham et al., 2007)
<i>ikaros</i>	(Willett et al., 2001)
<i>kdrl</i>	(Liang et al., 2001)
<i>pdgfrβ</i>	(Wiens et al., 2010)
<i>pu.1/spi1b</i>	(Jin et al., 2012)
<i>rag1</i>	(Willett et al., 1997)
<i>sox9a</i>	(Yan et al., 2002)

Phenotypic trait measurements

Phenotypic trait quantification was carried out on 2-5 clutches from confocal max projections or bright field images. All length measurements and miR-24 head size were obtained using Image J software (Schneider et al., 2012). For filopodia length and number quantification, at least 14 cells from 4 embryos per genotype were examined. The total length of ISVs, starting from the DA to the end of the growing vessel, was measured for at least 12 ISVs in four fish per genotype. ISV ectopic branch number was

obtained from 11 DMSO-treated and 21-26 GSI-treated embryos per condition. HA size was determined by the sum of several measurements along the entire vessel length including both branches that bifurcate from the central stem. HA length was evaluated for 5-6 miR-24 quadruple mutants and 12-18 embryos for other genotypes. Hemogenic endothelial cell and neutrophil counts were obtained for 17-24 and 30-50 embryos, respectively. Quantification of phenotypic variability was determined by the coefficient of variation calculation (Blevins et al., 2015; Felix and Barkoulas, 2015). Phenotypic trait values are directly represented in violin plots or were placed under a normal distribution to generate evidence based theoretical models.

miRNA target gene network analysis in endothelial cells

To identify the transcripts that could be targeted by miR-139, miR-24, and miR-223 in endothelial cells, mRNAs were isolated from a single replicate of FAC-sorted Kdr1:GFP⁺ 24 hpf-6 dpf endothelial cells by the poly(A)-capture protocol (Bazzini et al., 2012) and used to prepare libraries for deep sequencing according to the Illumina manufacturer's protocol. Trimmomatic processed sequencing reads were mapped to the Zv9 genome using Bowtie 2 (Langmead and Salzberg, 2012). Uniquely mapped reads were normalized using Cufflinks (Trapnell et al., 2012) to obtain Fragment Per Kilobase Of Exon Per Million Fragments Mapped (FPKM) analysis. 3'UTRs of genes with > 25 FPKM in at least one stage of development were analyzed by PITA (Kertesz et al., 2007), RNA22 (Miranda et al., 2006), and TargetScan v6.0 (Lewis et al., 2005; Ulitsky et al., 2012) programs for miRNA binding sites complementary to the seed regions of mature miR-139, miR-24, and miR-223 sequences. Genes identified by at least two of the prediction programs served as putative target genes for these miRNAs in endothelial cells. The Circos software package (Krzywinski et al., 2009) provided a genome-wide view of the identified miRNA target genes and their overall levels and differential gene expression patterns genes between cardiovascular developmental stages. Gene Ontology terms were assigned to target genes using the DAVID software (Huang da et al., 2009a, b). Classification of differentially expressed target genes as pro- and anti-angiogenic or hematopoietic effectors was based on previous literature. Interactions maps between each miRNA and these angiogenic or hematopoietic target genes were created using Cytoscape (Cline et al., 2007).

Primers

Primer name	F/R	Primer sequence (5'-3')	Assay
dre-miR-126	F	tcgtaccgtgagtaataatgc	qPCR
dre-miR-22a	F	aagctgccagctgaagaactgt	qPCR
dre-miR-139	F	tctacagtgcattgtctct	qPCR
dre-miR-150	F	tctccaatcctgtaccagtg	qPCR
dre-miR-223	F	tgtcagttgtcaaatacccc	qPCR
dre-miR-30b	F	tgtaaacatcctacactcagct	qPCR
dre-miR-30c	F	tgtaaacatcctacactctcagc	qPCR
dre-miR-30d	F	tgtaaacatccccgactggaag	qPCR
dre-miR-92a	F	tattgcactgtcccggcctgt	qPCR
dre-miR-99	F	aaccgtagatccgatctgtg	qPCR
dre-miR-128	F	tcacagtgaaccggctctcttt	qPCR
dre-miR-187	F	tcgtgtcttgtgttcagcc	qPCR
dre-miR-23a	F	atcacattgccagggtattcca	qPCR
dre-miR-24	F	tggtcagttcagcaggaacag	qPCR
dre-miR-27a	F	ttcacagtggctaagttccgct	qPCR
dre-miR-27b	F	ttcacagtggctaagttctgca	qPCR
dre-miR-27c	F	ttcacagtggtaagttctgc	qPCR
dre-miR-27d	F	ttcacagtggctaagttcttca	qPCR

dre-miR-27e	F	ttcacagtggctaagttcagtg	qPCR
dre-miR-125a	F	tcctgagaccctaacctgtg	qPCR
dre-miR-125b	F	tcctgagaccctaactgtga	qPCR
dre-let-7a	F	tgaggtagtaggtgtatagtt	qPCR
dre-let-7b	F	tgaggtagtaggtgtgtggtt	qPCR
dre-let-7c	F	tgaggtagtaggtgtatggtt	qPCR
dre-let-7d	F	tgaggtagtgggtgtatggtt	qPCR
dre-let-7e	F	tgaggtagtagattgaatagtt	qPCR
dre-let-7f	F	tgaggtagtagattgtatagtt	qPCR
dre-let-7g	F	tgaggtagtagttgtatagtt	qPCR
dre-let-7h	F	tgaggtagtaagttgtgtggtt	qPCR
dre-let-7i	F	tgaggtagtagttgtgctggtt	qPCR
dre-let-7j	F	tgaggtagtggttgtacagtt	qPCR
dre-cxcr4a	F	gggctcgtgatcctcatctg	qPCR
dre-cxcr4a	R	agcagacgatcagaaccacg	qPCR
dre-cmyb	F	tgctatccagagacactacagc	qPCR
dre-cmyb	R	agtgcctgtgtcccttcag	qPCR
dre-actb1	F	gatctggcatcacaccttctac	qPCR
dre-actb1	R	tcttctctgttggcttgg	qPCR
dre-miR-223	F	ccactcaaggtctcgcttt	genotyping
dre-miR-223	R	gagagtaacaggatcgcattg	genotyping
dre-miR-139	F	aagtgtagcttccggcttc	genotyping
dre-miR-139	R	gagccttagcctcagacttaac	genotyping
dre-miR-24-1	F	aagccatgaccaaggtaag	genotyping
dre-miR-24-1	R	ttgagacaaacacatcaagc	genotyping
dre-miR-24-2	F	tttccctctgtctgtgtct	genotyping
dre-miR-24-2	R	gtgaagggaagcgtccag	genotyping
dre-miR-24-3	F	ttgcacgggccgtattta	genotyping
dre-miR-24-3	R	tcctccatgaaggattgtc	genotyping
dre-miR-24-4	F	ctggtgctgatataggctctatg	genotyping
dre-miR-24-4	R	atcctcgtgccttgacttg	genotyping

Supplemental References

Bazzini, A.A., Lee, M.T., and Giraldez, A.J. (2012). Ribosome profiling shows that miR-430 reduces translation before causing mRNA decay in zebrafish. *Science* *336*, 233-237.

Blevins, R., Bruno, L., Carroll, T., Elliott, J., Marcais, A., Loh, C., Hertweck, A., Krek, A., Rajewsky, N., Chen, C.Z., *et al.* (2015). microRNAs regulate cell-to-cell variability of endogenous target gene expression in developing mouse thymocytes. *PLoS genetics* *11*, e1005020.

Bolger, A.M., Lohse, M., and Usadel, B. (2014). Trimmomatic: a flexible trimmer for Illumina sequence data. *Bioinformatics* *30*, 2114-2120.

Chong, S.W., Emelyanov, A., Gong, Z., and Korzh, V. (2001). Expression pattern of two zebrafish genes, *cxcr4a* and *cxcr4b*. *Mech Dev* *109*, 347-354.

Cline, M.S., Smoot, M., Cerami, E., Kuchinsky, A., Landys, N., Workman, C., Christmas, R., Avila-Campilo, I., Creech, M., Gross, B., *et al.* (2007). Integration of biological networks and gene expression data using Cytoscape. *Nature protocols* *2*, 2366-2382.

Dobin, A., Davis, C.A., Schlesinger, F., Drenkow, J., Zaleski, C., Jha, S., Batut, P., Chaisson, M., and Gingeras, T.R. (2013). STAR: ultrafast universal RNA-seq aligner. *Bioinformatics* *29*, 15-21.

Felix, M.A., and Barkoulas, M. (2015). Pervasive robustness in biological systems. *Nature reviews Genetics* *16*, 483-496.

Huang da, W., Sherman, B.T., and Lempicki, R.A. (2009a). Bioinformatics enrichment tools: paths toward the comprehensive functional analysis of large gene lists. *Nucleic acids research* *37*, 1-13.

Huang da, W., Sherman, B.T., and Lempicki, R.A. (2009b). Systematic and integrative analysis of large gene lists using DAVID bioinformatics resources. *Nature protocols* *4*, 44-57.

Jin, H., Li, L., Xu, J., Zhen, F., Zhu, L., Liu, P.P., Zhang, M., Zhang, W., and Wen, Z. (2012). Runx1 regulates embryonic myeloid fate choice in zebrafish through a negative feedback loop inhibiting Pu.1 expression. *Blood* *119*, 5239-5249.

Kertesz, M., Iovino, N., Unnerstall, U., Gaul, U., and Segal, E. (2007). The role of site accessibility in microRNA target recognition. *Nature genetics* *39*, 1278-1284.

Krzywinski, M., Schein, J., Birol, I., Connors, J., Gascoyne, R., Horsman, D., Jones, S.J., and Marra, M.A. (2009). Circos: an information aesthetic for comparative genomics. *Genome research* *19*, 1639-1645.

Langmead, B., and Salzberg, S.L. (2012). Fast gapped-read alignment with Bowtie 2. *Nature methods* *9*, 357-359.

Lewis, B.P., Burge, C.B., and Bartel, D.P. (2005). Conserved seed pairing, often flanked by adenosines, indicates that thousands of human genes are microRNA targets. *Cell* *120*, 15-20.

Liang, D., Chang, J.R., Chin, A.J., Smith, A., Kelly, C., Weinberg, E.S., and Ge, R. (2001). The role of vascular endothelial growth factor (VEGF) in vasculogenesis, angiogenesis, and hematopoiesis in zebrafish development. *Mech Dev* *108*, 29-43.

Miranda, K.C., Huynh, T., Tay, Y., Ang, Y.S., Tam, W.L., Thomson, A.M., Lim, B., and Rigoutsos, I. (2006). A pattern-based method for the identification of MicroRNA binding sites and their corresponding heteroduplexes. *Cell* *126*, 1203-1217.

- Moreno-Mateos, M.A., Vejnar, C.E., Beaudoin, J.D., Fernandez, J.P., Mis, E.K., Khokha, M.K., and Giraldez, A.J. (2015). CRISPRscan: designing highly efficient sgRNAs for CRISPR-Cas9 targeting in vivo. *Nature methods* 12, 982-988.
- Murayama, E., Kissa, K., Zapata, A., Mordelet, E., Briolat, V., Lin, H.F., Handin, R.I., and Herbomel, P. (2006). Tracing hematopoietic precursor migration to successive hematopoietic organs during zebrafish development. *Immunity* 25, 963-975.
- Ristori, E., Lopez-Ramirez, M.A., Narayanan, A., Hill-Teran, G., Moro, A., Calvo, C.F., Thomas, J.L., and Nicoli, S. (2015). A Dicer-miR-107 Interaction Regulates Biogenesis of Specific miRNAs Crucial for Neurogenesis. *Developmental cell* 32, 546-560.
- Schneider, C.A., Rasband, W.S., and Eliceiri, K.W. (2012). NIH Image to ImageJ: 25 years of image analysis. *Nature methods* 9, 671-675.
- Trapnell, C., Roberts, A., Goff, L., Pertea, G., Kim, D., Kelley, D.R., Pimentel, H., Salzberg, S.L., Rinn, J.L., and Pachter, L. (2012). Differential gene and transcript expression analysis of RNA-seq experiments with TopHat and Cufflinks. *Nature protocols* 7, 562-578.
- Ulitsky, I., Shkumatava, A., Jan, C.H., Subtelny, A.O., Koppstein, D., Bell, G.W., Sive, H., and Bartel, D.P. (2012). Extensive alternative polyadenylation during zebrafish development. *Genome research* 22, 2054-2066.
- Wiens, K.M., Lee, H.L., Shimada, H., Metcalf, A.E., Chao, M.Y., and Lien, C.L. (2010). Platelet-derived growth factor receptor beta is critical for zebrafish intersegmental vessel formation. *PLoS one* 5, e11324.
- Willett, C.E., Kawasaki, H., Amemiya, C.T., Lin, S., and Steiner, L.A. (2001). Ikaros expression as a marker for lymphoid progenitors during zebrafish development. *Developmental dynamics : an official publication of the American Association of Anatomists* 222, 694-698.
- Willett, C.E., Zapata, A.G., Hopkins, N., and Steiner, L.A. (1997). Expression of zebrafish rag genes during early development identifies the thymus. *Developmental biology* 182, 331-341.
- Yan, Y.L., Miller, C.T., Nissen, R.M., Singer, A., Liu, D., Kirn, A., Draper, B., Willoughby, J., Morcos, P.A., Amsterdam, A., *et al.* (2002). A zebrafish *sox9* gene required for cartilage morphogenesis. *Development* 129, 5065-5079.